Microbubbles for

Ultrasound-mediated Drug Delivery

Von der Medizinischen Fakultät
der Rheinisch-Westfälischen Technischen Hochschule Aachen
zur Erlangung des akademischen Grades einer Doktorin der Theoretischen Medizin
genehmigte Dissertation

vorgelegt von

Mengjiao Liu

aus Wuyang (China)

Berichter: Univ.-Prof. Dr. sc. hum. Twan Lammers
Priv.-Doz. Dr. rer. nat. Matthias Bartneck

Tag der mündlichen Prüfung: 15.01.2024

Diese Dissertation ist auf den Internetseiten der Universitätsbibliothek online verfügbar.

D 82 (Diss. RWTH Aachen University 2024)

Publikationsliste

Publikationen der Dissertation

Liu, M.*, Dasgupta, A.*, Qu, N., Rama, E., Kiessling, F. and Lammers, T., Strategies to Maximize Anthracycline Drug Loading in Albumin Microbubbles. *ACS Biomaterials Science and engineering*, 2021, https://doi.org/10.1021/acsbiomaterials.1c01203.

Liu, M.*, Dasgupta, A.*, Koczera, P., Schipper, S., Rommel, D., Shi, Y., Kiessling, F. and Lammers, T., Drug Loading in Poly(butyl cyanoacrylate)-Based Polymeric Microbubbles. *Molecular Pharmaceutics*, 2020, *17*(8), pp.2840-2848.

Weitere Publikationen

Fernandes, A.C.*, **Liu, M.***, Sorbo, T., Appold, L.C., Ilbert, M., Ferracci, G., Kiessling, F., F Branco, R.J., Lammers, T. and Iranzo, O., A computational and experimental study to develop E-selectin targeted peptides for molecular imaging applications. *Future medicinal chemistry*, 2018, *10*(23), pp.2695-2711.

Dasgupta, A., **Liu, M.**, Ojha, T., Storm, G., Kiessling, F. and Lammers, T., Ultrasound-mediated drug delivery to the brain: principles, progress and prospects. *Drug Discovery Today: Technologies*, 2016, *20*, pp.41-48.

Koczera P., Appold L., Shi Y., **Liu M.**, Dasgupta A., Pathak V., Ojha T., Fokong S., Wu Z., van Zandvoort M., Iranzo O., Kuehne AJC., Pich A., Kiessling F., Lammers T., PBCA-based polymeric microbubbles for molecular imaging and drug delivery. *Journal of Controlled Release*, 259 (2017), pp. 128-135

Dasgupta, A., Sun, T., Palomba, R., Rama, E., Zhang, Y., Power, C., Moeckel, D., **Liu, M.**, Sarode, A., Weiler, M. and Motta, A., Nonspherical ultrasound microbubbles. *Proceedings of the National Academy of Sciences*, 2023, 120(13), p.e2218847120.

molecular pharmaceutics

pubs.acs.org/molecularpharmaceutics

Article

Drug Loading in Poly(butyl cyanoacrylate)-Based Polymeric Microbubbles

Mengjiao Liu,[‖] Anshuman Dasgupta,[‖] Patrick Koczera, Sandra Schipper, Dirk Rommel, Yang Shi, Fabian Kiessling, and Twan Lammers*

Cite This: *Mol. Pharmaceutics* 2020, 17, 2840−2848

Read Online

ACCESS | Metrics & More | Article Recommendations | Supporting Information

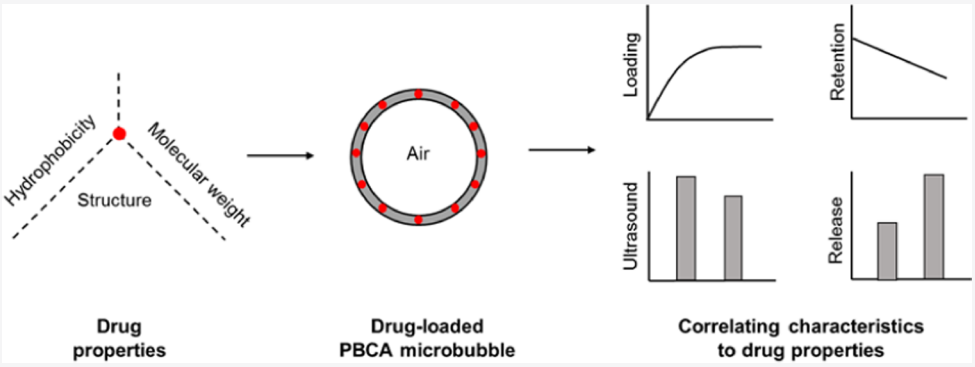

ABSTRACT: Microbubbles (MB) are routinely used ultrasound (US) contrast agents that have recently attracted increasing attention as stimuli-responsive drug delivery systems. To better understand MB-based drug delivery, we studied the role of drug hydrophobicity and molecular weight on MB loading, shelf-life stability, US properties, and drug release. Eight model drugs, varying in hydrophobicity and molecular weight, were loaded into the shell of poly(butyl cyanoacrylate) (PBCA) MB. In the case of drugs with progesterone as a common structural backbone (i.e., for corticosteroids), loading capacity and drug release correlated well with hydrophobicity and molecular weight. Conversely, when employing drugs with no structural similarity (i.e., four different fluorescent dyes), loading capacity and release did not correlate with hydrophobicity and molecular weight. All model drug-loaded MB formulations could be equally efficiently destroyed upon exposure to US. Together, these findings provide valuable insights on how the physicochemical properties of (model) drug molecules affect their loading and retention in and US-induced release from polymeric MB, thereby facilitating the development of drug-loaded MB formulations for US-triggered drug delivery.

KEYWORDS: *drug delivery, theranostics, microbubbles, ultrasound, PBCA, corticosteroids*

1. INTRODUCTION

Microbubbles (MB) are 1−10 μm sized air-filled vesicles that are shell-stabilized by lipids, proteins, or polymers. They are widely used as contrast agents for functional and molecular ultrasound (US) imaging.[1−3] Apart from US imaging, MB have recently gained increasing attention for drug delivery purposes: when MB are exposed to US, they oscillate (at low mechanical index) or implode (at high mechanical index), resulting in a number of biophysical phenomena, which are known to permeabilize blood vessel and cellular membranes, thereby facilitating drug delivery into tissues and cells.[4−10]

In the context of MB- and US-mediated drug delivery, strategies have focused on both coadministration and coformulation, the former being applied more frequently so far.[11−13] This may be due to the fact that coformulation is somewhat more demanding since it requires the loading of drugs or drug delivery systems into or onto the MB shell.[14,15] A particular advantage of using drug-loaded MB is that upon US exposure, drug release from the MB shell is specifically facilitated at a target site, thereby improving efficacy, while at the same time reducing off-target drug localization and side effects. This strategy has shown promise in thrombolysis and tumor therapy.[16]

For coformulation, polymer-based hard shell MB have advantages compared to lipid-based soft shell MB, as they can encapsulate higher amounts of drug molecules in their much thicker shell.[17,18] Among polymers used for MB synthesis, poly(butyl cyanoacrylate) (PBCA) is a well known and biocompatible polymer that is synthesized via the anionic

Received: March 5, 2020
Revised: June 25, 2020
Accepted: June 26, 2020
Published: June 26, 2020

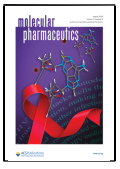

https://dx.doi.org/10.1021/acs.molpharmaceut.0c00242
Mol. Pharmaceutics 2020, 17, 2840−2848

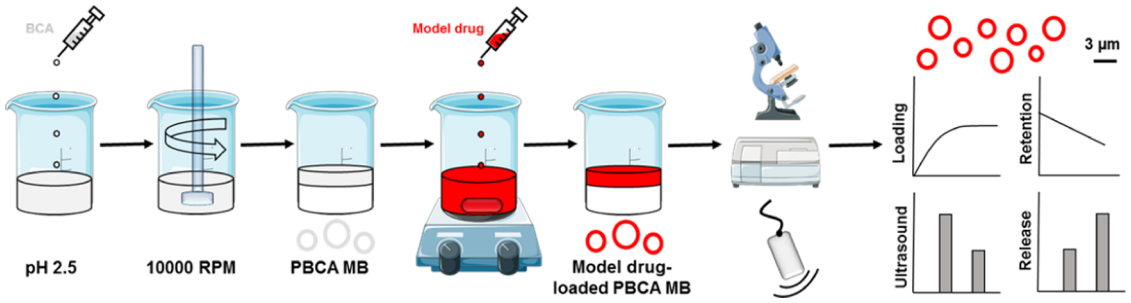

Figure 1. Schematic study setup. Poly(butyl cyanoacrylate)-based (PBCA) polymeric microbubbles (MB) were synthesized by the anionic polymerization of BCA. Upon loading of eight different (model) drugs into the shell of PBCA MB, several characterization techniques were employed to study drug loading capacity, drug retention, ultrasound (US) properties, and US-induced drug release.

Corticosteroids	Structure	Hydrophobicity (Log P)	Molecular weight (Da)
Dexamethasone	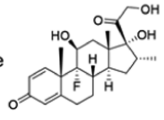	1.7	392.5
Budesonide	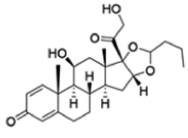	2.4	430.5
Halcinonide	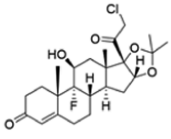	3.3	455.0
Ciclesonide	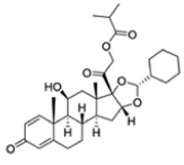	4.1	540.7

Dyes	Structure	Hydrophobicity (Log P)	Molecular weight (Da)
Rhodamine B	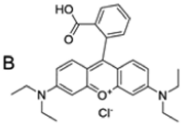	2.4	479.0
Nile red	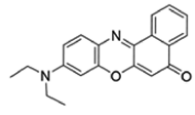	3.5	318.4
Coumarin 6	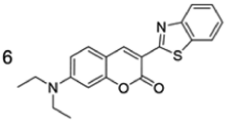	4.9	350.4
Pyrene	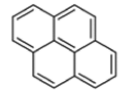	6.0	202.3

Figure 2. Overview of the (model) drugs used in this study. Corticosteroids with progesterone as a common structural derivative (whose hydrophobicity and molecular weight increased simultaneously; left panel) and fluorescent dyes with no common structural derivative (whose hydrophobicity and molecular weight did not increase simultaneously; right panel) were loaded into the shell of PBCA MB.

polymerization and that has been used not only for MB preparation but also for generating chemotherapy-loaded nanoparticles, several of which have even made it to evaluation in patients.[19] Moreover, Sulheim et al. showed that nanoparticles made of PBCA can be internalized and efficiently degraded inside cells, potentially facilitating intracellular drug release. However, longer alkyl side-chain cyanoacrylates, as in poly(octyl cyanoacrylate) nanoparticles, remained intact. This notion supports the use of PBCA as a polymeric material for drug delivery applications.[20,21] Previously, we showed that PBCA MB could efficiently encapsulate ultrasmall superparamagnetic iron oxide (USPIO) nanoparticles, as well as fluorophores such as rhodamine B and coumarin 6 into the polymeric shell.[22,23] Wheatley and colleagues found that paclitaxel, a highly hydrophobic drug, was encapsulated in the polymeric shell more efficiently than doxorubicin, which is more hydrophilic.[24] However, systematic investigations on how drug properties influence drug loading into and drug release from the shell of polymeric MB are lacking, which is essential for translating such systems to the clinic.

In this paper, we set out to better understand the effect of drug hydrophobicity (i.e., log *P*) and molecular weight on the loading, stability, US properties, and drug release profile of PBCA MB. To this end, we loaded eight different model drugs into the shell of PBCA MB and characterized the resulting formulations using spectroscopy, high-performance liquid chromatography (HPLC), and US imaging (Figure 1). We observed that for corticosteroids with progesterone as a common structural derivative (Figure 2, left panel), loading capacity and release correlated with concurrently increasing hydrophobicity and molecular weight. For structurally different dyes, whose hydrophobicity and molecular weight did not concurrently increase (Figure 2, right panel), loading capacity and release did not correlate with hydrophobicity and molecular weight. These findings provide important new insights on how drug properties affect the loading, stability, US properties, and release of polymeric MB, which may facilitate the development of drug-loaded MB formulations.

https://dx.doi.org/10.1021/acs.molpharmaceut.0c00242
Mol. Pharmaceutics 2020, 17, 2840−2848

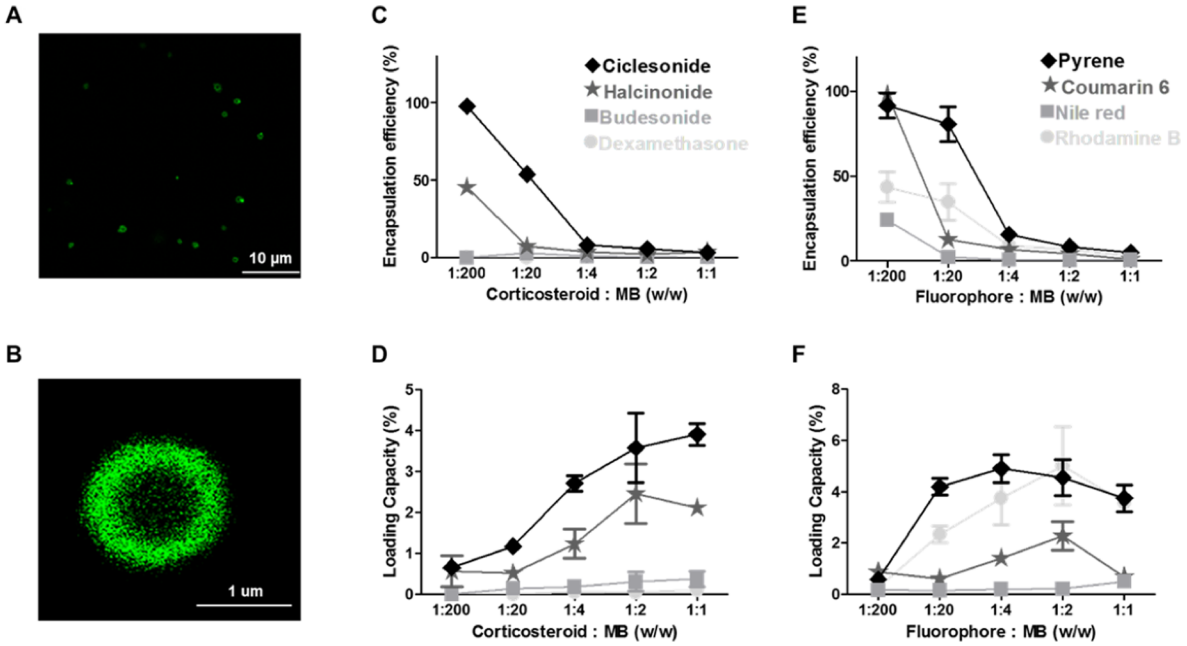

Figure 3. Loading capacity and encapsulation efficiency of PBCA MB. (A, B) Representative fluorescence microscopy image exemplifying successful loading of coumarin 6 into the shell of PBCA MB. (C, D) Quantification of corticosteroids in MB showing that an increase in hydrophobicity and molecular weight results in an increased encapsulation efficiency and loading capacity. (E, F) Quantitative analysis of fluorophore-loaded MB showing that with increasing hydrophobicity, loading capacity and encapsulation efficiency also tend to increase, with the exception of rhodamine B. Note that the color-coding of the plotted lines corresponds to the degree of hydrophobicity. Values represent mean ± standard deviation of three different batches of drug-loaded MB, measured in triplicates.

2. MATERIALS AND METHODS

2.1. Materials. Butyl cyanoacrylate (BCA) was purchased from Special Polymer Ltd. (Bulgaria). Dexamethasone, budesonide, coumarin 6, pyrene, Nile red, Triton X-100, gelatin, dimethyl sulfoxide (DMSO), acetonitrile (ACN), and methanol were bought from Sigma-Aldrich (Germany). Halcinonide was obtained from United States Pharmacopeia (Italy) and rhodamine B from AppliChem GmbH (Germany). Deionized (DI) water was used for all experiments and all other reagents were of appropriate analytical grade.

2.2. Synthesis of PBCA-Based Polymeric MB. Poly(butyl cyanoacrylate) (PBCA) MB were synthesized using a previously established protocol.[22,25] Briefly, 3 mL of BCA monomer was added dropwise to 300 mL of an aqueous solution containing 1% (w/v) Triton X-100 at pH 2.5. Upon dropwise addition of BCA, the mixture was homogenized at 10 000 rpm for 1 h using an Ultra-Turrax (IKA-Werke, Germany). This led to the formation of air-filled polydispersed MB. Subsequently, these MB were purified by multiple centrifugation steps at 500 rpm for 20 min and were finally suspended in 0.02% (w/v) Triton X-100 at pH 7. These purification steps resulted in a relatively monodispersed MB size population with a mean size of approximately 2.5 μm.[13,22]

2.3. Quantification of Size, Size Distribution, and Concentration of PBCA MB. The size distribution and concentration of PBCA MB were analyzed using a Multisizer 3 (Beckmann Coulter, Germany), which was equipped with a 30 μm sensor orifice. Briefly, 20 mL of an isotonic solution was poured into a cuvette and was placed on the sample platform. This was used as a blank measurement to correct for background noise. Subsequently, 10 μL of PBCA MB was diluted with 20 mL of the isotonic solution and the sample was measured in a volumetric mode with a dilution factor of 2000. These steps were repeated in triplicates to obtain mean ± standard deviation.

2.4. Drug Loading into the Shell of PBCA-Based Polymeric MB. The corticosteroids, dexamethasone, budesonide, halcinonide, and ciclesonide, and the fluorescent dyes, rhodamine B, nile red, coumarin 6, and pyrene were used as model compounds for studying drug loading into the shell of PBCA-based polymeric MB. Different (model) drug amounts, i.e., 0.1, 1, 5, 10, and 20 mg, were dissolved in 200 μL of DMSO and subsequently mixed in 10 mL of an aqueous suspension containing 10^{10} MB. These drug amounts corresponded to the feed ratios (drug/MB) w/w of 1:200, 1:20, 1:4, 1:2, and 1:1, respectively. The mixtures were stirred at 250 rpm for 19 h at room temperature (RT). To remove the unloaded drug, the MB were allowed to float due to their buoyant force, and the aqueous solution underneath the MB was replaced multiple times until there was no free drug present anymore.[13] Finally, the drug-loaded MB were suspended in 0.02% (w/v) Triton X-100 at pH 7 and stored at RT for further characterization.

2.5. Confocal Laser Scanning Microscopy. Coumarin 6 was utilized to visualize encapsulation in the shell of PBCA MB. A Leica TCS SP8 X inverted confocal microscope (Leica Microsystems, Wetzlar, Germany) equipped with a plan-apochromat 100×/1.40 oil-immersion objective was used to visualize coumarin 6 loading in PBCA MB. The samples were applied on a high-precision cover glass (170 μm, no. 1.5H) from Marienfeld (Lauda-Königshofen, Germany). The excitation wavelength was set at λ = 470 nm via a filtered white light laser, and the resulting emission was detected at λ = 491−556 nm. Deconvolution of the images was processed using the Huygens Professional software via the classic maximum likelihood estimation (CMLE) method.

2.6. Quantification of Drug Loading. All samples were prepared by diluting 10 μL of drug-loaded MB with 90 μL of

https://dx.doi.org/10.1021/acs.molpharmaceut.0c00242
Mol. Pharmaceutics 2020, 17, 2840−2848

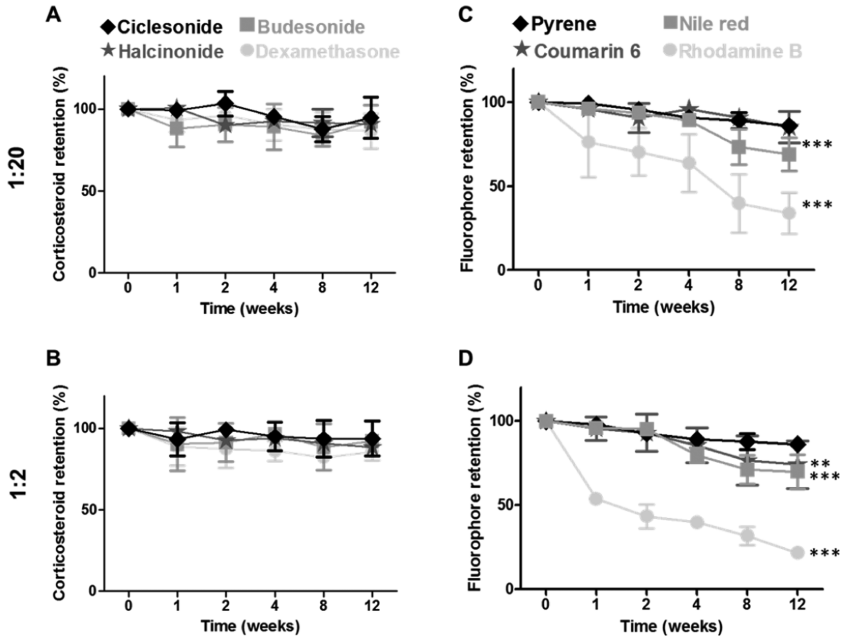

Figure 4. Shelf-life stability of drug-loaded PBCA MB. (A, B) Quantitative analysis of drug retention, showing that at both the 1:20 and 1:2 feed ratios, corticosteroid content did not decrease significantly over time and exemplifying that all four drugs were efficiently retained in the MB shell even after 12 weeks of storage. (C, D) Quantitative analysis of fluorophore retention showing that fluorescent dyes were less efficiently retained at the higher feed ratio of 1:2 as compared to lower feed ratio of 1:20. Additionally, less hydrophobic model drugs were less efficiently retained in the MB shell and vice-versa. Note that the color-coding of the plotted lines corresponds to the degree of hydrophobicity. Values represent mean ± standard deviation of three different batches of drug-loaded MB, measured in triplicates. All statistical comparisons were made with respect to week 0. $^{**}p < 0.01$ and $^{***}p < 0.001$.

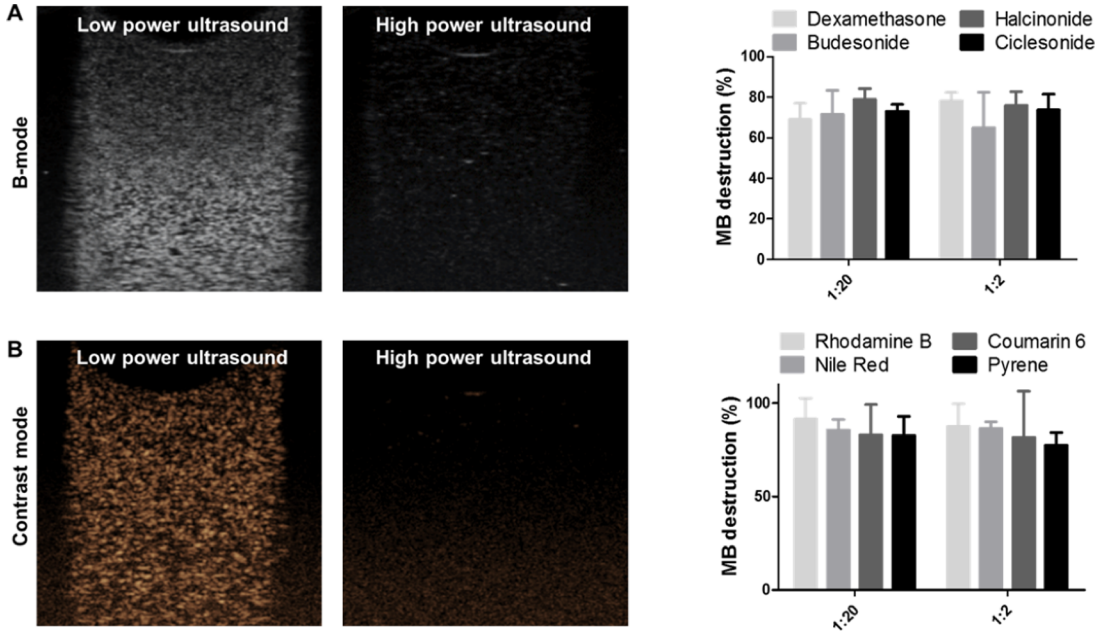

Figure 5. Ultrasound analysis of drug-loaded PBCA MB. (A, B) Representative B-mode and contrast-mode images of all drug-loaded PBCA MB showing that ultrasound (US) contrast is efficiently generated at low powers, while at high powers, MB are destroyed (as evidenced by the lack of US contrast). (C, D) Quantitative analysis of MB destruction showing that there are no significant differences between the different drug-loaded PBCA MB, and demonstrating that US properties are independent of the hydrophobicity and molecular weight of the encapsulated drug. Note that the color-coding of the plotted lines corresponds to the degree of hydrophobicity. Values represent mean ± standard deviation of three different batches of drug-loaded MB, measured in triplicates.

DMSO, which destroyed the MB and facilitated the release of the encapsulated model drugs. The amount of drug incorporated into the MB shell was then quantified either using a microplate reader TECAN Infinite M200 Pro (Tecan Group Ltd., Germany) or high-performance liquid chromatography (HPLC). The details of the experimental parameters used in the plate reader and HPLC are summarized in Table S1. Finally, encapsulation efficiency (EE) and loading capacity (LC) of all

https://dx.doi.org/10.1021/acs.molpharmaceut.0c00242
Mol. Pharmaceutics 2020, 17, 2840−2848

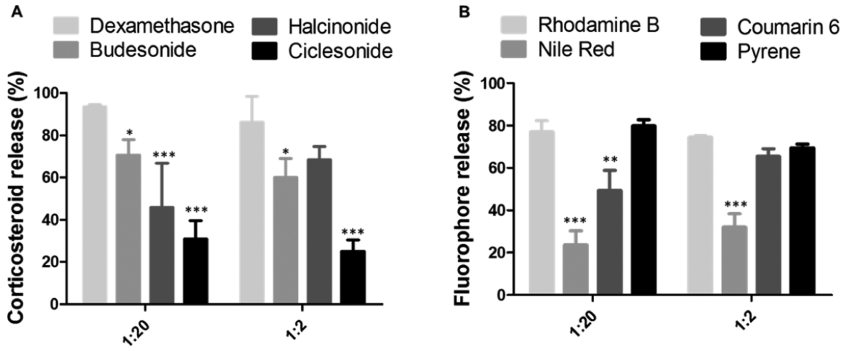

Figure 6. US-induced drug release from PBCA MB. (A) Quantitative analysis of corticosteroid release showing that hydrophobicity and molecular weight negatively affect US-induced drug release. (B) Fluorophore release from the MB shell did not show a relationship with hydrophobicity and molecular weight. Note that color-coding corresponds to the degree of hydrophobicity. Values represent mean ± standard deviation of three different batches of drug-loaded MB, measured in triplicates. All statistical comparisons were made with respect to dexamethasone and rhodamine B in (A) and (B), respectively. *$p < 0.05$, **$p < 0.01$, and ***$p < 0.001$.

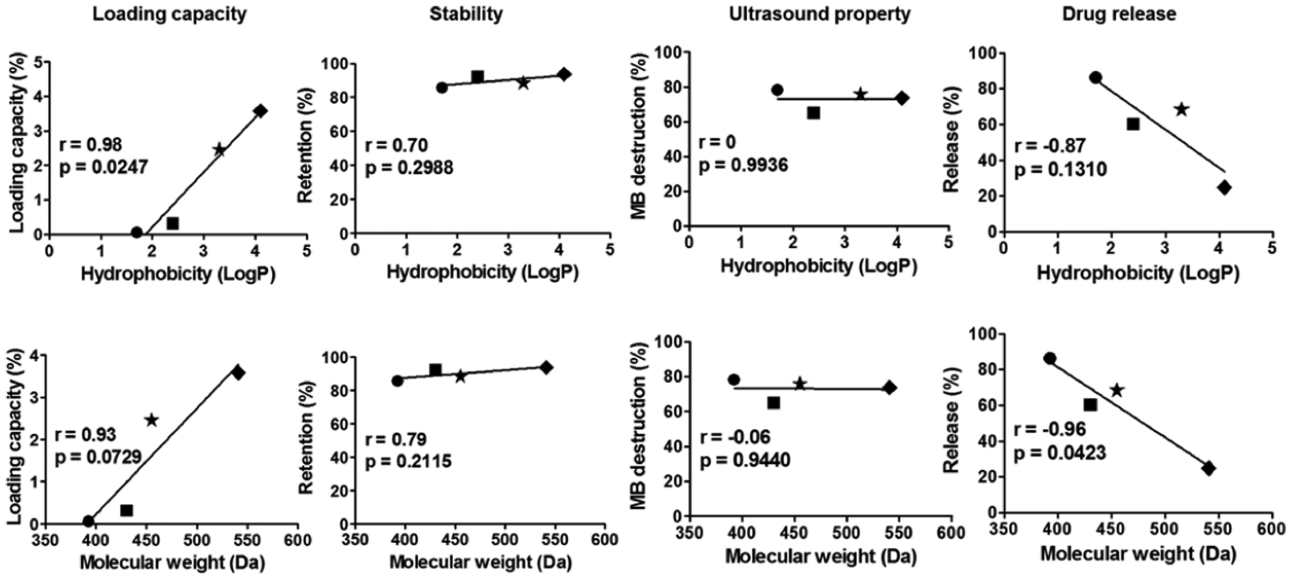

Figure 7. Correlating the hydrophobicity (top) and molecular weight (bottom) of corticosteroid drugs with the characteristics of shell-loaded PBCA MB. Loading capacity and drug release of corticosteroid-loaded MB showed a good correlation with both hydrophobicity and molecular weight. Symbols: ● = dexamethasone; ■ = budesonide; ★ = halcinonide; ◆ = ciclesonide.

MB formulations were determined using the formulas: EE = (weight of drug incorporated/weight of drug added during the formulation) × 100%; and LC = (weight of drug incorporated/weight of drug-loaded MB) × 100%.

2.7. Stability Assessment of Drug-Loaded MB. MB formulations containing 10^9 MB/mL (i.e., a relevant range for in vivo application; equivalent to 2 mg/mL) were stored in screw-cap glass vials at RT for stability analysis. In particular, retention of drugs inside the MB shell was studied over a period of 12 weeks and quantified using the formula: drug retention at week x = (amount of drug retained inside the MB shell at week x/amount of incorporated drug) × 100%.

2.8. US Analysis of Drug-Loaded MB. To study the effect of drug encapsulation on US properties, MB with and without model drugs were exposed to low- and high-power US, and based on these responses, the percentage of MB destruction was quantified. For this purpose, 3×10^5 MB were suspended in 4.5 mL of a 2% w/v gelatin solution, and the mixture was embedded in a 10% w/v gelatin solution. A preclinical US device (Vevo 2100, VisualSonics, Canada) was employed to image the MB in gelatin phantoms. US imaging was performed in a nonlinear contrast mode at a center frequency of 18 MHz, initially with 4% power (mechanical index 0.2), followed by 100% power (mechanical index 0.9) to destroy the MB in the gelatin phantom. A region-of-interest (ROI) of approximately 500 mm^2 was drawn at the middle of all images, and the resulting contrast intensity was analyzed using the Vevo LAB software. Finally, % MB destruction was quantified as: ((US contrast at 4% power − US contrast at 100% power)/US contrast at 4% power) × 100%.

2.9. Quantification of US-Mediated Drug Release. An ultrasonic cleaner device (UCS 200TH, VWR) was employed to destroy the MB and to induce the release of encapsulated model drugs from the MB shell.[22,26] To ensure that all of the released model drugs were retained in the supernatant, we diluted 10^9 MB with 0.02% (w/v) Triton X-100 such that the final drug concentration was lower than its solubility. All MB samples were subjected to US for 10 min. The samples were subsequently centrifuged at 10 000 rpm for 10 min to separate the polymer fragments (as a result of MB destruction) from the released drugs (supernatant). The amount of released drugs was quantified in a similar way as described in Section 2.4, and

https://dx.doi.org/10.1021/acs.molpharmaceut.0c00242
Mol. Pharmaceutics 2020, 17, 2840−2848

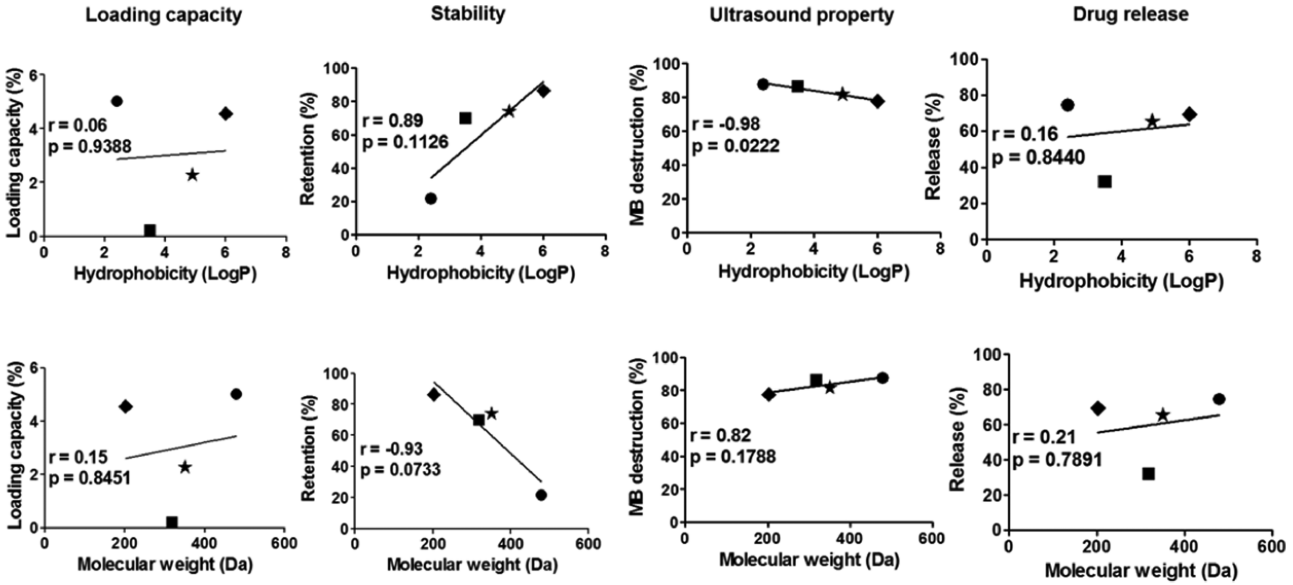

Figure 8. Correlating hydrophobicity (top) and molecular weight (bottom) of fluorophores with the characteristics of shell-loaded PBCA MB. Only shelf-life stability showed a good correlation with both hydrophobicity and molecular weight. Symbols: ● = rhodamine B; ■ = nile red; ★ = coumarin 6; ◆ = pyrene.

upon analyses, drug release was determined as the percentage of the total encapsulated drug.

2.10. Statistical Analysis. Three different batches of drug-loaded MB formulations were prepared from three different batches of preformed MB, and each formulation was measured thrice. All values are presented as mean ± standard deviation. Statistical analyses were performed using GraphPad Prism 5. The results in Figures 3−6 were analyzed using two-way ANOVA, corrected for multiple comparisons (Bonferroni). The correlation analyses in Figures 7 and 8 were performed using Pearson's r coefficients. A p value of less than 0.05 was considered to be statistically significant.

3. RESULTS AND DISCUSSION

3.1. Loading Capacity and Encapsulation Efficiency of PBCA MB. We loaded four different corticosteroids and four different fluorescent dyes into the shell of PBCA MB (Figure 2). As a proof-of-concept, Figure 3A,B shows that the fluorescent model drug coumarin 6 can indeed be successfully loaded into the shell of PBCA MB. We furthermore evaluated five different feed ratios, i.e., 1:200, 1:20, 1:4, 1:2, and 1:1, to achieve maximal levels of drug amounts inside the MB shell. We observed that model drug loading at different feed ratios does not influence the size and size distribution of PBCA MB (see Figure S1 and Table S2).

The selected corticosteroids had progesterone as a common structural backbone, and their hydrophobicity and molecular weight increased simultaneously. Upon loading them into the shell of PBCA MB, we observed that as the hydrophobicity of these drugs increased, MB payload increased. This is shown in Figure 3C, where dexamethasone, budesonide, halcinonide, and ciclesonide, in the order of increasing hydrophobicity, resulted in increasing encapsulation efficiencies, e.g., at a 1:20 feed ratio, values of 0.02, 2.75, 7.05, and 53.86% were obtained. Similarly, at a feed ratio of 1:2, corticosteroid loading capacity increased in the order of increasing hydrophobicity, with values of 0.05, 0.31, 2.46, and 3.58%, respectively (Figure 3D). These values were significantly different from each other ($p < 0.001$) except when comparing the two least hydrophobic drugs, i.e., dexamethasone versus budesonide. Analogously, since hydrophobicity and molecular weight concurrently increased for corticosteroids that had common progesterone backbone, employing these molecules with increasing molecular weight also led to an increase in MB loading.

On the other hand, the fluorescent dyes selected for this study were structurally different, and their hydrophobicity and molecular weight did not increase in the same order. Their order of increasing hydrophobicity was rhodamine B, nile red, coumarin 6, and pyrene, while their order of increasing molecular weight was pyrene, nile red, coumarin 6, and rhodamine B (see Figure 2). When studying the impact of hydrophobicity on MB payload, Figure 3E,F demonstrates that increasing hydrophobicity led to an increase in encapsulation efficiency and loading capacity, with the exception of rhodamine B. Rhodamine B, which was the least hydrophobic dye, was still encapsulated quite efficiently into the MB shell. This may be due to the relatively large molecular weight of rhodamine B, allowing for more efficient retention in the PBCA shell even after several washing steps during the experiment. Similarly, and along the same line of thinking, fluorescent dyes with increasing molecular weight were more efficiently retained and loaded into the MB shell, with the exception of pyrene. Pyrene, being the smallest in molecular weight, was still efficiently loaded into the PBCA shell, as it was the most hydrophobic dye molecule (Figure 3E,F).

These findings can also be explained from a structural point of view. PBCA has a carbonyl oxygen and a cyanate nitrogen, which are both partially electronegatively charged, making it possible to have an n−π^* type of interaction in which they donate electron-ion pairs to electropositive sites in corticosteroids and dyes.[27] For corticosteroids, the four drugs used in this study had a similar progesterone-based structural backbone, the only variations being in substitutions of the exocyclic side chains. The presence of such substituted groups can change the electronegativity of neighboring molecules and thus influence its interaction with PBCA. Examples of this are the presence of fluorine in dexamethasone versus hydrogen in budesonide, or

https://dx.doi.org/10.1021/acs.molpharmaceut.0c00242
Mol. Pharmaceutics 2020, 17, 2840−2848

the presence of the hydroxyl group in dexamethasone versus a diether group in the other corticosteroids. Along the same line of thinking, also increasing the side chain (as in ciclesonide) resulted in increased affinity toward PBCA. As opposed to the steroids, for the dyes, the molecular structures greatly differed. All have a benzene ring subunit, which provides free electrons for exchange and interaction with the MB shell. Coumarin 6 has more free electrons than Nile red, which potentially explains its enhanced interaction with PBCA. Rhodamine B not only has free and flexible electrons in its rings but also contains electropositively charged oxygen, which may interact with both carbonyl oxygen and cyanate nitrogen on the PBCA,[28] and which potentially explain its relatively efficient loading.

The results in Figure 3 and the above molecular interactions directly relate to the shell composition of PBCA MB, which is highly hydrophobic and has a thickness of 50−200 nm,[13] thereby allowing hydrophobic drug molecules to be incorporated efficiently. Smaller molecular weight drugs are likely washed out of the PBCA MB shell more easily than larger molecular weight drugs during the washing steps, explaining the more efficient retention and higher loading of larger molecular weight drug molecules. Similar findings have been reported for poly(lactic acid) (PLA)-based MB, which were shown to encapsulate paclitaxel, a hydrophobic and relatively large anticancer drug more efficiently than doxorubicin, which is less hydrophobic and smaller.[24] Overall, these findings indicate that the loading of PBCA MB increases with increasing drug hydrophobicity and molecular weight.

3.2. Shelf-Life Stability of Drug-Loaded PBCA MB. We employed the formulations that had minimal and maximal levels of drug molecules in the MB shell for the analysis of shelf-life stability, US properties, and drug release. Given the negligible differences and similar amounts of drugs were loaded for the 1:200 and 1:20 feed ratios, we opted to use the 1:20 feed ratio as the minimal one. For the maximal one, saturated levels of drug amounts were observed at the 1:2 feed ratio.

For stability studies, MB formulations were stored at RT and drug retention was quantified over a period of 1, 2, 4, 8, and 12 weeks. We observed only very minute changes (<5%) in the size of MB formulations after 12 weeks of storage (see Table S3). In the case of corticosteroids, there was no statistically significant decline in drug retention over time at a feed ratio of 1:20 ($p > 0.05$; Figure 4A), exemplifying that all four drugs were efficiently retained in the MB shell even after 12 weeks of storage. Similar findings were also observed at the 1:2 feed ratio (Figure 4B), highlighting that all corticosteroid-loaded MB were stable up to 12 weeks upon storage at RT. Importantly, these experiments only demonstrate proper shelf-life stability of drug-loaded MB. To be able to draw conclusions on stable in vivo drug retention in the shell of PBCA MB, experiments in more complex media (e.g., in full-blood or serum) are needed.

As opposed to the corticosteroid case, fluorophore retention varied quite a bit with the feed ratio and hydrophobicity. Figure 4C,D shows that fluorophores at a higher feed ratio (i.e., 1:2) are less efficiently retained in the MB shell than those at a lower feed ratio (i.e., 1:20). In the context of hydrophobicity, fluorophores with low hydrophobicity were found to be poorly retained in the MB shell. This is illustrated in Figure 4C, showing that rhodamine B, nile red, coumarin 6, and pyrene, in the order of increasing hydrophobicity, gave rise to more efficient dye retention upon 12 weeks of storage, with values of 33.97% ($p < 0.001$), 68.94% ($p < 0.001$), 85.12% ($p > 0.05$), and 85.85% ($p > 0.05$), respectively. Conversely, fluorophore retention in the MB shell did not depend on the fluorophore molecular weight (Figure 4C,D). Together, these analyses demonstrate that all corticosteroids were efficiently retained in the MB shell. In the case of fluorophores, retention in the MB shell increased with dye hydrophobicity.

3.3. US Properties of Drug-Loaded PBCA MB. To study the US properties of the MB formulations upon drug encapsulation, they were embedded in tissue-mimicking gelatin phantoms and exposed to US. Figure 5A,B shows representative US B-mode and contrast-mode images, respectively, illustrating that all drug-loaded MB generated contrast at low-power US and were efficiently destroyed at high-power US.

In the case of corticosteroid-loaded MB, there were no differences in the extent of MB destruction between the four formulations ($p > 0.05$; Figure 5C), exemplifying that the destruction of the MB was independent of the hydrophobicity and molecular weight of the encapsulated drug. Analogously, also in the case of the dye-loaded MB, the destruction levels were similar for rhodamine B, nile red, coumarin 6, and pyrene-loaded MB (independent of the feed ratio; $p > 0.05$; Figure 5D). One plausible explanation is that due to the relatively low loading capacity of PBCA MB (<5%), the overall effect of molecular interactions between the loaded agents and the PBCA shell is not very substantial.

Overall, it can be concluded that drug-loaded MB can be efficiently destroyed by US, indicating that drug loading does not negatively affect MB response to US. Additionally, all drug-loaded MB were equally efficient in getting destroyed upon US exposure, highlighting that the destruction of MB formulations has no dependency on the properties of the model drug.

3.4. US-Induced Drug Release from PBCA MB. For corticosteroids, US-induced drug release from the MB shell decreased as the hydrophobicity of the drug increased. This is exemplified in Figure 6A for the 1:20 feed ratio, with dexamethasone, budesonide, halcinonide, and ciclesonide—in the order of increasing hydrophobicity—showing release percentages of 93.62, 70.64, 45.99, and 30.81%, respectively. All of these values were significantly lower than dexamethasone. Similarly, US-induced drug release was decreased as the molecular weight of the corticosteroid increased. Also at the 1:2 feed ratio, these drugs with lower hydrophobicity and smaller molecular weight were more efficiently released from the MB shell (Figure 6A). These findings can be explained by taking the thick and hydrophobic shell of PBCA MB into account, which allows for a stronger interaction with more hydrophobic and larger molecular weight drugs, eventually resulting in less efficient release as compared to for hydrophilic and smaller molecular weight drugs.

In the case of the fluorophores, increasing hydrophobicity of the encapsulated model drugs did not result in any clear relationship with drug release from the MB shell (Figure 6B). Similarly, also when studying the effect of model drug molecular weight on its US-induced release from the MB shell, there appeared no clear relationship (Figure 6B). In summary, for corticosteroids with a common progesterone backbone, triggered drug release was inversely correlated with hydrophobicity and molecular weight. Vice versa, for structurally different fluorescent dyes, drug release did not show any relationship with hydrophobicity and molecular weight.

3.5. Correlating Drug Hydrophobicity and Molecular Weight with PBCA MB Characteristics. Taking all of the above results together, we finally correlated both hydrophobicity and molecular weight of the selected (model) drugs with key

https://dx.doi.org/10.1021/acs.molpharmaceut.0c00242
Mol. Pharmaceutics 2020, 17, 2840−2848

characteristics of resulting MB formulations, i.e., with loading capacity, shelf-life stability, US properties, and US-induced drug release at the 1:2 feed ratio. In the case of corticosteroids, which had progesterone as a common structural backbone and whose hydrophobicity and molecular weight increased concurrently, several key characteristics showed a good correlation with both hydrophobicity and molecular weight. This is exemplified in Figure 7, illustrating that loading capacity correlated reasonably well with hydrophobicity (r = 0.98) and molecular weight (r = 0.93). Also, drug release correlated relatively well with hydrophobicity (r = −0.87) and molecular weight (r = −0.96), but in an inverse manner. Two of these correlations were of borderline insignificance, which can be due to the relatively low sample size.

Also, the shelf-life stability correlates relatively well with hydrophobicity and molecular weight, but the almost horizontal slope shows that the overall impact is very small. US properties did not correlate with hydrophobicity and molecular weight (Figure 7). These findings are favorable because it shows that independent of drug properties, drug entrapment in the MB shell is stable. Corticosteroid-loaded MB such as the ones described here may find applications in priming tumors for improved delivery of drugs and drug delivery systems by permeabilizing tumor vessels via the oscillation of MB and at the same time reducing the extent of extracellular matrix deposition in tumors through the release and action of corticosteroids.[29,30]

In the case of the fluorophores, which were structurally very different and whose hydrophobicity and molecular weight did not increase concurrently, most characteristics studied did not show a good correlation with hydrophobicity and molecular weight. This is depicted in Figure 8, exemplifying that loading capacity and drug release did not correlate with the hydrophobicity and molecular weight (r < 0.2). MB destructibility did correlate with hydrophobicity and molecular weight, but the overall impact seems minimal since the slope is close to horizontal. Only the shelf-life stability of fluorophore-loaded MB correlated well with hydrophobicity (r = 0.89) and molecular weight (r = −0.93) of the encapsulated dyes. In general, fluorophore-loaded MB may find application in different multimodal imaging setups, for instance in experiments aiming to verify the in vivo binding of ligand-targeted MB to tumor or inflamed blood vessels in an ex vivo microscopy setup, or in studies looking at the ex vivo distribution of polymer shell fragments at pathological (target) sites after US-mediated MB destruction.[13,31−33]

4. CONCLUSIONS

We show that PBCA-based polymeric MB can be used to encapsulate a variety of model drugs. For drugs with progesterone as a common structural derivative, we found that compounds with increasing hydrophobicity and molecular weight can be loaded and retained more efficiently in the shell of PBCA MB but are less efficiently released upon US-mediated MB destruction. Conversely, when employing structurally different fluorescent dyes, loading capacity and compound release did not correlate with hydrophobicity and molecular weight. Taking everything together, the results presented here demonstrate that the physicochemical properties of (model) drugs play an important role in determining loading in and release from PBCA-based MB.

■ ASSOCIATED CONTENT

Supporting Information

The Supporting Information is available free of charge at https://pubs.acs.org/doi/10.1021/acs.molpharmaceut.0c00242.

Size distribution of unloaded and drug-loaded PBCA MB, experimental parameters used in the spectroscopy and HPLC analyses, size of unloaded and drug-loaded PBCA MB, and size of drug-loaded PBCA MB over time (PDF)

■ AUTHOR INFORMATION

Corresponding Author

Twan Lammers − *Institute for Experimental Molecular Imaging, RWTH Aachen University Clinic, Aachen 52074, Germany;* orcid.org/0000-0002-1090-6805; Email: tlammers@ukaachen.de

Authors

Mengjiao Liu − *Institute for Experimental Molecular Imaging, RWTH Aachen University Clinic, Aachen 52074, Germany*

Anshuman Dasgupta − *Institute for Experimental Molecular Imaging, RWTH Aachen University Clinic, Aachen 52074, Germany*

Patrick Koczera − *Institute for Experimental Molecular Imaging and Department of Intensive Care Medicine, Medical Faculty, RWTH Aachen University Clinic, Aachen 52074, Germany*

Sandra Schipper − *Institute for Experimental Molecular Imaging, RWTH Aachen University Clinic, Aachen 52074, Germany*

Dirk Rommel − *DWI—Leibniz Institute for Interactive Materials, RWTH Aachen University, Aachen 52074, Germany*

Yang Shi − *Institute for Experimental Molecular Imaging, RWTH Aachen University Clinic, Aachen 52074, Germany;* orcid.org/0000-0003-4530-2056

Fabian Kiessling − *Institute for Experimental Molecular Imaging, RWTH Aachen University Clinic, Aachen 52074, Germany;* orcid.org/0000-0002-7341-0399

Complete contact information is available at: https://pubs.acs.org/10.1021/acs.molpharmaceut.0c00242

Author Contributions

‖M.L. and A.D. contributed equally.

Notes

The authors declare no competing financial interest.

■ ACKNOWLEDGMENTS

The authors gratefully acknowledge the financial support from the Chinese Scholarship Council (grant number 201506910070), the European Commission (EuroNanoMed-III: NSC4DIPG), the European Research Council (ERC-CoG 864121), and the German Research Foundation (DFG: GRK2375 (grant #331065168), SFB1066 and SFB/TRR57). Image templates from Servier Medical Art (http://smart.servier.com) were used for the preparation of Figure 1.

■ REFERENCES

(1) Lindner, J. R. Microbubbles in medical imaging: current applications and future directions. *Nat. Rev. Drug Discovery* **2004**, *3*, 527−532.

(2) Klibanov, A. L. Ligand-carrying gas-filled microbubbles: ultrasound contrast agents for targeted molecular imaging. *Bioconjugate Chem.* **2005**, *16*, 9−17.

(3) Kiessling, F.; Huppert, J.; Palmowski, M. Functional and molecular ultrasound imaging: concepts and contrast agents. *Curr. Med. Chem.* **2009**, *16*, 627−642.
(4) Unger, E. C.; Hersh, E.; Vannan, M.; Matsunaga, T. O.; McCreery, T. Local drug and gene delivery through microbubbles. *Prog. Cardiovasc. Dis.* **2001**, *44*, 45−54.
(5) Mitragotri, S. Healing sound: the use of ultrasound in drug delivery and other therapeutic applications. *Nat. Rev. Drug Discovery* **2005**, *4*, 255−260.
(6) Dasgupta, A.; Liu, M.; Ojha, T.; Storm, G.; Kiessling, F.; Lammers, T. Ultrasound-mediated drug delivery to the brain: principles, progress and prospects. *Drug Discovery Today: Technol.* **2016**, *20*, 41−48.
(7) Frenkel, V. Ultrasound mediated delivery of drugs and genes to solid tumors. *Adv. Drug Delivery Rev.* **2008**, *60*, 1193−1208.
(8) Hernot, S.; Klibanov, A. L. Microbubbles in ultrasound-triggered drug and gene delivery. *Adv. Drug Delivery Rev.* **2008**, *60*, 1153−1166.
(9) Lentacker, I.; De Smedt, S. C.; Sanders, N. N. Drug loaded microbubble design for ultrasound triggered delivery. *Soft Matter* **2009**, *5*, 2161−2170.
(10) Klibanov, A. L.; Shevchenko, T. I.; Raju, B. I.; Seip, R.; Chin, C. T. Ultrasound-triggered release of materials entrapped in microbubble-liposome constructs: a tool for targeted drug delivery. *J. Controlled Release* **2010**, *148*, 13−17.
(11) Deckers, R.; Yudina, A.; Cardoit, L. C.; Moonen, C. T. A fluorescent chromophore TOTO-3 as a 'smart probe' for the assessment of ultrasound-mediated local drug delivery in vivo. *Contrast Media Mol. Imaging* **2011**, *6*, 267−274.
(12) Treat, L. H.; McDannold, N.; Vykhodtseva, N.; Zhang, Y.; Tam, K.; Hynynen, K. Targeted delivery of doxorubicin to the rat brain at therapeutic levels using MRI-guided focused ultrasound. *Int. J. Cancer* **2007**, *121*, 901−907.
(13) Koczera, P.; Appold, L.; Shi, Y.; Liu, M.; Dasgupta, A.; Pathak, V.; Ojha, T.; Fokong, S.; Wu, Z.; van Zandvoort, M.; Iranzo, O.; Kuehne, A. J. C.; Pich, A.; Kiessling, F.; Lammers, T. PBCA-based polymeric microbubbles for molecular imaging and drug delivery. *J. Controlled Release* **2017**, *259*, 128−135.
(14) Liang, X.; Xu, Y.; Gao, C.; Zhou, Y. M.; Zhang, N. S.; Dai, Z. F. Ultrasound contrast agent microbubbles with ultrahigh loading capacity of camptothecin and floxuridine for enhancing tumor accumulation and combined chemotherapeutic efficacy. *NPG Asia Mater.* **2018**, *10*, 761−774.
(15) Chen, P. Y.; Yeh, C. K.; Hsu, P. H.; Lin, C. Y.; Huang, C. Y.; Wei, K. C.; Liu, H. L. Drug-carrying microbubbles as a theranostic tool in convection-enhanced delivery for brain tumor therapy. *Oncotarget* **2017**, *8*, 42359−42371.
(16) Gong, Q.; Gao, X.; Liu, W.; Hong, T.; Chen, C. Drug-Loaded Microbubbles Combined with Ultrasound for Thrombolysis and Malignant Tumor Therapy. *BioMed Res. Int.* **2019**, No. 6792465.
(17) Cavalieri, F.; Zhou, M.; Tortora, M.; Lucilla, B.; Ashokkumar, M. Methods of Preparation of Multifunctional Microbubbles and their In Vitro/In Vivo Assessment of Stability, Functional and Structural Properties. *Curr. Pharm. Des.* **2012**, *18*, 2135−2151.
(18) Sirsi, S. R.; Borden, M. A. Microbubble compositions, properties and biomedical applications. *Bubble Sci., Eng., Technol.* **2009**, *1*, 3−17.
(19) Zhou, Q.; Sun, X.; Zeng, L.; Liu, J.; Zhang, Z. Randomized Multicenter Phase II Clinical Trial of Mitoxantrone-Loaded Nanoparticles in the Treatment of 108 Patients with Unresected Hepatocellular Carcinoma. *Nanomedicine* **2009**, *5*, 419−423.
(20) El-Egakey, M. A.; Bentele, V.; Kreuter, J. Molecular Weights of Polycyanoacrylate Nanoparticles. *Int. J. Pharm.* **1983**, *13*, 349−352.
(21) Sulheim, E.; Baghirov, H.; von Haartman, E.; Bøe, A.; Åslund, A. K.; Mørch, Y.; de Lange Davies, C. Cellular uptake and intracellular degradation of poly (alkyl cyanoacrylate) nanoparticles. *J. Nanobiotechnol.* **2016**, *14*, No. 1.
(22) Fokong, S.; Theek, B.; Wu, Z.; Koczera, P.; Appold, L.; Jorge, S.; Resch-Genger, U.; van Zandvoort, M.; Storm, G.; Kiessling, F.; Lammers, T. Image-guided, targeted and triggered drug delivery to tumors using polymer-based microbubbles. *J. Controlled Release* **2012**, *163*, 75−81.
(23) Liu, Z.; Lammers, T.; Ehling, J.; Fokong, S.; Bornemann, J.; Kiessling, F.; Gätjens, J. Iron oxide nanoparticle-containing microbubble composites as contrast agents for MR and ultrasound dual-modality imaging. *Biomaterials* **2011**, *32*, 6155−6163.
(24) Cochran, M. C.; Eisenbrey, J.; Ouma, R. O.; Soulen, M.; Wheatley, M. A. Doxorubicin and paclitaxel loaded microbubbles for ultrasound triggered drug delivery. *Int. J. Pharm.* **2011**, *414*, 161−170.
(25) Fokong, S.; Siepmann, M.; Liu, Z.; Schmitz, G.; Kiessling, F.; Gatjens, J. Advanced characterization and refinement of poly N-butyl cyanoacrylate microbubbles for ultrasound imaging. *Ultrasound Med. Biol.* **2011**, *37*, 1622−1634.
(26) Appold, L.; Shi, Y.; Rütten, S.; Kühne, A.; Pich, A.; Kiessling, F.; Lammers, T. Physicochemical Characterization of the Shell Composition of PBCA-Based Polymeric Microbubbles. *Macromol. Biosci.* **2017**, *17*, No. 1700002.
(27) Yang, S. C.; Ge, H. X.; Hu, Y.; Jiang, X. Q.; Yang, C. Z. Formation of positively charged poly (butyl cyanoacrylate) nanoparticles stabilized with chitosan. *Colloid Polym. Sci.* **2000**, *278*, 285−292.
(28) Wan, Y.; Wang, X.; Gu, Y.; Guo, L.; Xu, Z. Surface-binding through polyfunction groups of Rhodamine B on composite surface and its high performance photodegradation. *Appl. Surf. Sci.* **2016**, *366*, 59−66.
(29) Barnes, P. J. How corticosteroids control inflammation: quintiles prize lecture 2005. *Br. J. Pharmacol.* **2006**, *148*, 245−254.
(30) Zhang, L.; Su, H.; Liu, Y.; Pang, N.; Li, J.; Qi, X. R. Enhancing solid tumor therapy with sequential delivery of dexamethasone and docetaxel engineered in a single carrier to overcome stromal resistance to drug delivery. *J. Controlled Release* **2019**, *294*, 1−16.
(31) Liu, Z.; Koczera, P.; Doleschel, D.; Kiessling, F.; Gatjens, J. Versatile synthetic strategies for PBCA-based hybrid fluorescent microbubbles and their potential theranostic applications to cell labelling and imaging. *Chem. Commun.* **2012**, *48*, 5142−5144.
(32) Koczera, P.; Wu, Z.; Fokong, S.; Theek, B.; Appold, L.; Jorge, S.; Möckel, D.; Liu, Z.; Curaj, A.; Storm, G.; van Zandvoort, M.; Kiessling, F.; Lammers, T. Fluorescently labeled microbubbles for facilitating translational molecular ultrasound studies. *Drug Delivery Transl. Res.* **2012**, *2*, 56−64.
(33) Fernandes, A. C.; Liu, M.; Sorbo, T.; Appold, L.; Ilbert, C. M.; Ferracci, G.; Kiessling, F.; Branco, R. J. F.; Lammers, T.; Iranzo, O. A computational and experimental study to develop E-selectin targeted peptides for molecular imaging applications. *Future Med. Chem.* **2018**, *10*, 2695−2711.

https://dx.doi.org/10.1021/acs.molpharmaceut.0c00242
Mol. Pharmaceutics 2020, 17, 2840−2848

- Supplementary information -

Figure S1

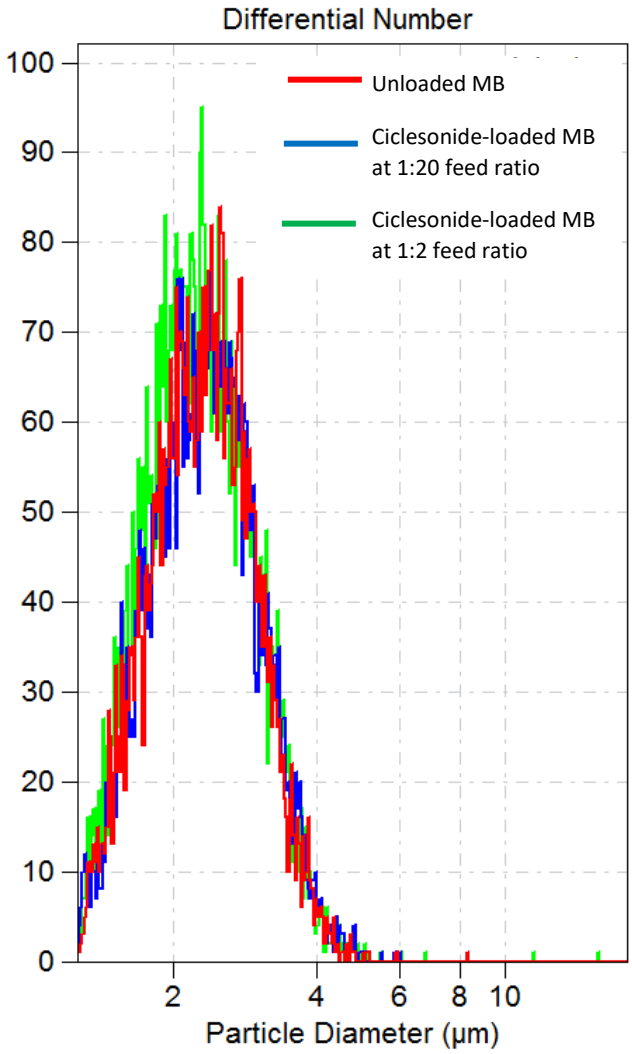

Figure S1. Size distribution of unloaded and drug-loaded PBCA MB. Qualitative analysis showing that model drug loading into the MB shell does not influence the size distribution of PBCA MB.

Table S1

Drug	Parameter
Dexamethasone	ACN:H_2O = 35:65 (0.01 % H_3PO_4, pH = 1.89), 240 nm, 1 ml/min, 200 ul
Budesonide	ACN:H_2O = 35:65 (0.01 % H_3PO_4, pH = 1.89), 240 nm, 1 ml/min, 200 ul
Halcinonide	Methanol (0.01%TFA):H_2O = 65:35, 220 nm, 1 ml/min, 200 ul
Ciclesonide	Methanol (0.1%TFA):H_2O = 95:5, 242 nm, 1 ml/min, 200 ul
Rhodamine B	Excitation Wavelength 548 nm, Emission Wavelength 590 nm
Coumarin 6	Excitation Wavelength 467 nm, Emission Wavelength 514 nm
Nile red	Excitation Wavelength 548 nm, Emission Wavelength 634 nm
Pyrene	Excitation Wavelength 332 nm, Emission Wavelength 384 nm

Table S1. Experimental parameters used in the spectrocopy and HPLC analyses.

Figure S2

Batches	Size of unloaded MB (µm)	Size of budesonide-loaded MB (µm)		Size of ciclesonide-loaded MB (µm)	
		Feed ratio 1:20	Feed ratio 1:2	Feed ratio 1:20	Feed ratio 1:2
Batch 1	2.358	2.387	2.363	2.399	2.339
Batch 2	2.554	2.547	2.615	2.572	2.527
Batch 3	2.755	2.801	2.764	2.812	2.835

Table S2. Size of unloaded and drug-loaded PBCA MB. Quantitative analysis showing that model drug loading into the MB shell does not influence the size of PBCA MB.

Figure S3

Budesonide-loaded MB	Feed ratio	Size (µm)					
		Week 0	Week 1	Week 2	Week 4	Week 8	Week 12
Batch 1	1:20	2.387	2.378	2.32	2.327	2.339	2.307
	1:2	2.363	2.332	2.476	2.307	2.307	2.254
Batch 2	1:20	2.547	2.558	2.363	2.481	2.495	2.449
	1:2	2.615	2.587	2.345	2.554	2.538	2.493
Batch 3	1:20	2.801	2.767	2.788	2.746	2.777	2.752
	1:2	2.764	2.806	2.78	2.792	2.748	2.695

Ciclesonide-loaded MB	Feed ratio	Size (µm)					
		Week 0	Week 1	Week 2	Week 4	Week 8	Week 12
Batch 1	1:20	2.399	2.374	2.377	2.355	2.333	2.325
	1:2	2.339	2.305	2.274	2.26	2.3	2.241
Batch 2	1:20	2.572	2.559	2.473	2.448	2.463	2.474
	1:2	2.527	2.478	2.446	2.438	2.481	2.401
Batch 3	1:20	2.812	2.804	2.795	2.76	2.708	2.656
	1:2	2.835	2.815	2.821	2.682	2.789	2.692

Table S3. Size of drug-loaded PBCA MB over time. Quantitative analysis showing that size of model drug-loaded PBCA MB changed very minutely (< 5 %) after 12 weeks of storage.

ACS Biomaterials SCIENCE & ENGINEERING

pubs.acs.org/journal/abseba

Article

Strategies to Maximize Anthracycline Drug Loading in Albumin Microbubbles

Mengjiao Liu,[†] Anshuman Dasgupta,[†] Na Qu, Elena Rama, Fabian Kiessling, and Twan Lammers*

Cite This: https://doi.org/10.1021/acsbiomaterials.1c01203

Read Online

ACCESS | Metrics & More | Article Recommendations | Supporting Information

ABSTRACT: Human serum albumin (HSA) microbubbles (MBs) are attracting increasing attention as image-guided and stimuli-responsive drug delivery systems. To better understand and maximize drug encapsulation in HSA MBs, we investigated the impact of the loading strategy and the drugs' physicochemical properties on their entrapment in the MB shell. Regarding loading strategy, we explored preloading, i.e., incubating drugs with HSA prior to MB formation, as well as postloading, i.e., incubating drugs with preformed MB. Both strategies were utilized to encapsulate six anthracyclines with different physicochemical properties. We demonstrate that drug loading in the HSA MB shell profits from preloading as well as from employing drugs with high intrinsic HSA binding affinity. These findings exemplify the potential of exploiting the natural bioconjugation interactions between drugs and HSA to formulate optimally loaded MBs, and they promote the development of HSA MBs for ultrasound-triggered drug delivery.

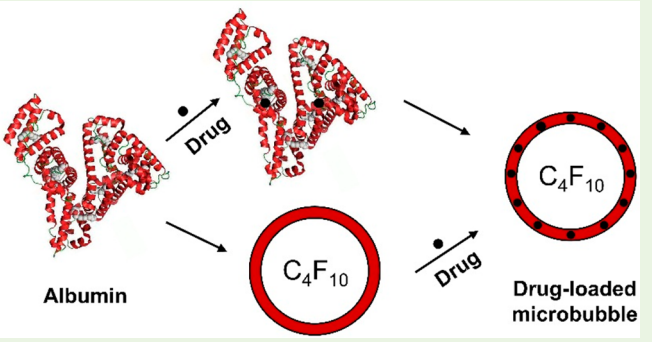

KEYWORDS: *drug delivery, albumin binding, human serum albumin, microbubbles, ultrasound*

INTRODUCTION

Microbubbles (MBs) are 1−10 μm sized air-filled vesicles whose shell is stabilized by polymers, proteins, or lipids.[1−3] MBs are routinely used in the clinic as ultrasound (US) contrast agents and they are also increasingly employed for drug delivery purposes.[4−10] When MBs are combined with US, they oscillate and/or implode, resulting in shear forces near (endothelial) cell membranes that cause permeabilization and opening of cell−cell contacts.[11] These phenomenona can contribute to improved delivery and efficacy of coadministered drugs.[6] However, administering free drugs in combination with MBs and US results in off-target drug localization and side effects.

Drug loading in MBs has been gaining more and more attention to avoid off-target localization and enable triggered drug release at the pathological site upon US-mediated MB destruction.[12−14] Drugs can be loaded either into a lipid, protein, or polymer shell-based MBs. Lipid-based MBs cannot be efficiently shell-loaded because of their relatively thin shell (<5 nm)[2]. Conversely, polymer- and protein-based MBs enable more efficient drug loading because of their much thicker shell (20−200 nm)[2]. In the case of polymeric MBs, we showed that drug loading in the shell of poly(butylcyanoacrylate)-based polymeric MBs is maximized by employing a two-step loading strategy, i.e., incubating preformed MBs with drugs, and by employing drugs with high hydrophobicity and molecular weight.[15,16] A downside of polymeric MBs is that they are currently not yet used in the clinic. On the other hand, human serum albumin (HSA)-based protein MBs such as Optison are available off-the-shelf and therefore developing drug-loaded HSA MBs may be easier to translate in the short term.[17,18] However, systematic studies on how factors like loading strategies and drug physicochemical properties impact drug loading into the shell of HSA-based protein MBs are lacking. These studies would provide an understanding that can enable efficient drug encapsulation in the shell of HSA MBs, which is important for the development and clinical translation of drug-loaded HSA MBs.

We investigated the impact of the drug loading strategies and the drugs' physicochemical properties on the efficiency of drug encapsulation in the shell of HSA MBs. We explored preloading, i.e., incubating HSA with drugs prior to MB synthesis, as well as postloading, i.e., incubating preformed HSA MBs with drugs (Figure 1A). To systematically study drug loading in HSA MBs, we employed six anthracyclines, i.e., idarubicin, daunorubicin, doxorubicin, epirubicin, pirarubicin, and valrubicin. These anthracyclines varied in their binding

Special Issue: Bioconjugates

Received: September 21, 2021
Accepted: December 9, 2021

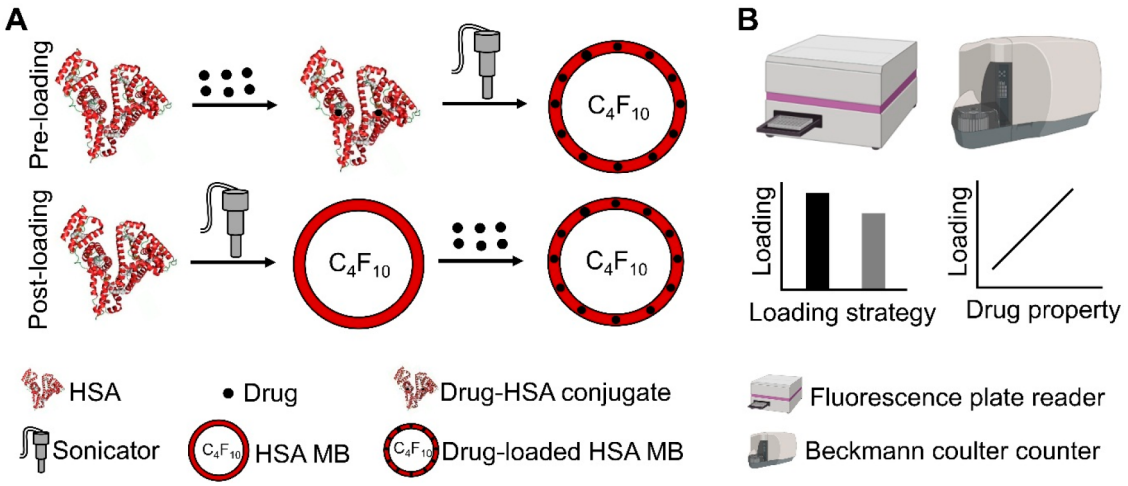

Figure 1. Experimental design. (A) Two different loading strategies, i.e., preloading and postloading, were explored to encapsulate drugs into the shells of HSA MBs with maximum efficiency. (B) Drug-loaded HSA MBs were characterized by fluorescence spectroscopy and Coulter counter-based sizing to study the impact of the different loading strategies and the drugs' physicochemical properties on the loading into the shells of HSA MBs. Created with BioRender.com.

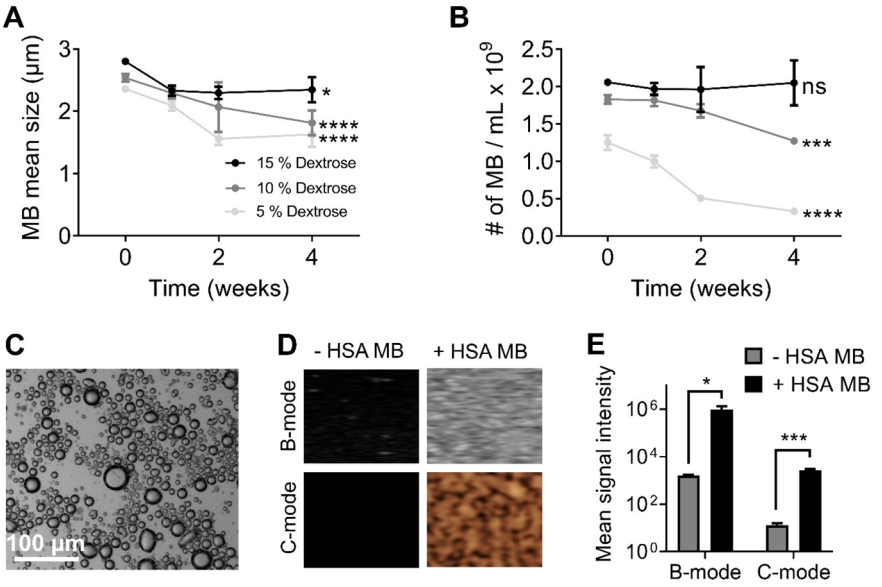

Figure 2. Formulation strategies to obtain long-term stable HSA MBs. (A, B) Quantitative analysis of MB stability showing that 15% (w/v) dextrose resulted in the least significant change in (A) the mean size and (B) the concentration of HSA MBs upon 4 weeks of storage at room temperature. (C) Representative light microscopy image demonstrating that HSA MBs synthesized using 15% (w/v) dextrose is spherically shaped and relatively polydisperse. (D, E) Ultrasound (US) (D) images and (E) quantification revealed that HSA MBs generated a significantly higher brightness-mode (B-mode) and contrast-mode (C-mode) US signal as compared to an aqueous solution without MBs. Data represent mean ± standard deviation for three different batches of non-drug-loaded HSA MBs. Statistical comparisons were performed between week 0 and week 4 for A and B. For E, statistical comparisons were performed between the control and HSA MB. *, ***, and **** represent $p < 0.05$, $p < 0.001$, and $p < 0.0001$, respectively.

percentages to albumin, their hydrophobicities, and their molecular weights. We characterized the resulting drug-loaded HSA MBs using fluorescence spectroscopy and Coulter counter-based sizing (Figure 1B). We hypothesized that drug loading in the shell of HSA MBs can be enhanced by preloading and by employing drugs with a high albumin binding affinity. The results obtained highlight the importance of both the loading strategy and the drugs' physicochemical properties on encapsulation in HSA MBs, and they are essential for the successful therapeutic use of drug-loaded HSA MB formulations.

RESULTS AND DISCUSSIONS

To develop drug-loaded HSA MB, we first identified experimental factors that affect the formation and long-term stability of US-responsive HSA MBs. Dextrose is a sugar molecule that has been shown to prevent coalescence and to stabilize HSA MB dispersions.[3,19] We therefore initially tested dextrose concentrations of 5, 10, and 15% weight/volume (% w/v) to obtain stable HSA MBs. For this purpose, we added the dextrose to HSA, and the mixture was subsequently sonicated to obtain HSA MB formulations. After preparation, we studied the stability of HSA MBs by storing them at room

https://doi.org/10.1021/acsbiomaterials.1c01203
ACS Biomater. Sci. Eng. XXXX, XXX, XXX−XXX

Table 1. Physicochemical Properties of the Anthracyclines Used in the Study[a]

Anthracycline	Structure	Drug bound to albumin (%)	Hydrophobicity (Log P)	Molecular weight (Da)
Idarubicin	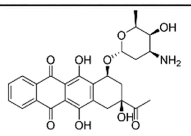	32.3 ± 7.6	1.6	497.5
Daunorubicin	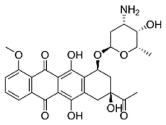	52.2 ± 4.7	1.6	527.5
Doxorubicin	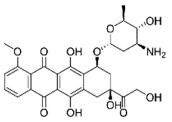	55.4 ± 4.8	1.4	543.5
Epirubicin	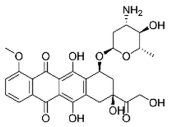	65.4 ± 1.7	1.4	543.5
Pirarubicin	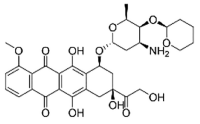	81.9 ± 6.8	2.0	627.6
Valrubicin	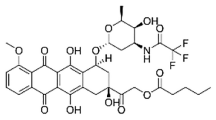	92.8 ± 2.1	2.2	723.6

[a]Idarubicin, daunorubicin, doxorubicin, epirubicin, pirarubicin, and valrubicin, which have varying binding percentages to albumin, hydrophobicity, and/or molecular weight were loaded into the shell of HSA MB. Binding percentage to albumin of the anthracyclines were determined experimentally and presented as mean ± standard deviation of three independent experiments. Hydrophobicity (log *P*) values were obtained from https://go.drugbank.com/.

temperature (RT) and by evaluating their mean size and concentration for a period of 4 weeks.

We observed that 5 and 10% (w/v) dextrose was not sufficient to form stable HSA MBs, as the mean size and concentration of HSA MBs were significantly reduced after 4 weeks of storage ($p < 0.001$, Figure 2A,B). Conversely, 15% (w/v) dextrose gave rise to relatively stable HSA MBs, with mean sizes reduced to a lesser extent ($p < 0.05$), and with no change in the concentration of HSA MBs over time ($p > 0.05$). We next characterized the HSA MBs obtained upon formulation at 15% (w/v) dextrose in terms of their physicochemical and US characteristics. Bright-field microscopy exemplified that HSA MBs were spherical in shape (Figure 2C) and Coulter counter results showed that they were relatively polydispersed (Figure S1), with a mean size and concentration of 2.4 ± 0.2 μm and 1.3 ± 0.2 × 10^9 MB/mL, respectively. Concerning US properties, panels D and E in Figure 2 revealed that HSA MBs efficiently generated US contrast in both brightness-mode (B-mode) and contrast-mode (C-mode). Together, these findings indicate that sonicating a mixture of 15% (w/v) dextrose and HSA results in the formation of spherical-shaped and relatively stable HSA MBs that generate good US contrast. In the following, we therefore focused on 15% (w/v) dextrose as a dispersion medium for the development of drug-loaded HSA MB formulations.

We subsequently studied the impact of the drug loading strategy and physicochemical properties on the efficiency of drug loading into the shell of HSA MBs. We explored both preloading, i.e., incubating the drugs with HSA prior to MB formation, and postloading, i.e., incubating drugs with preformed HSA MBs. Six structurally and functionally similar anthracyclines with somewhat different physicochemical properties (i.e., the drug binding percentage to albumin, the hydrophobicity, and the molecular weight) were employed (Table 1). Furthermore, we evaluated two different drug to albumin feed ratios, i.e. 1:1 and 2:1, to saturate the drug binding pockets of HSA and to thereby maximize drug loading into HSA MBs.

When studying the impact of the loading strategy, light microscopy photographic images of anthracycline-loaded MB formulations demonstrated that preloading resulted in a higher color intensity in the floating MB cakes, indicating more efficient anthracycline loading (Figure 3A). Indeed, at a 1:1 feed ratio, the one-step preloading strategy resulted in significantly higher loading of valrubicin into the HSA MB shell as compared to the two-step postloading strategy (Figure 3B). In line with this, the other five anthracyclines employed also showed higher drug loading efficiency for preloading, but in these cases, the differences were not statistically significant (Figure 3B).

https://doi.org/10.1021/acsbiomaterials.1c01203
ACS Biomater. Sci. Eng. XXXX, XXX, XXX−XXX

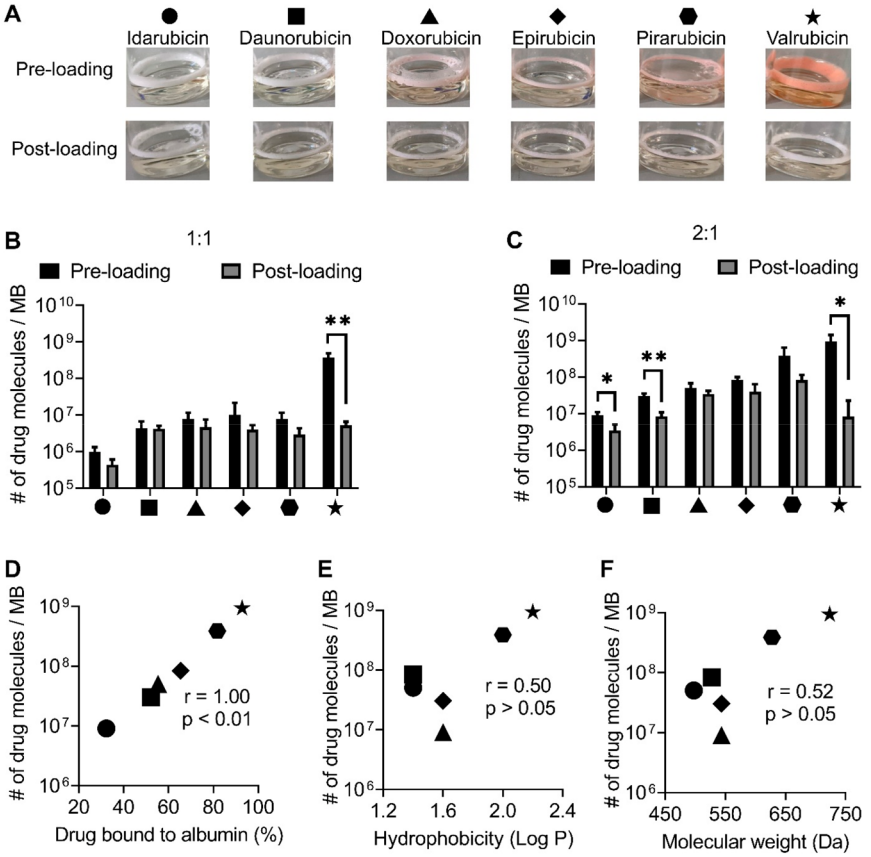

Figure 3. Impact of the drug loading strategy and the drugs' physicochemical properties on anthracycline loading into HSA MBs. (A) Preloading resulted in a higher intensity color in floating MBs compared to postloading. (B, C) Quantification of the amount of drug molecules in the HSA MB shell upon pre- and postloading at 1:1 and 2:1 feed ratios. (D) Anthracycline loading into the HSA MB shell correlated very well with binding percentage to albumin. (E, F) Anthracycline loading did not correlate with hydrophobicity and molecular weight. Data represent the mean ± standard deviation for three different batches of drug-loaded HSA MB. Statistical comparisons were performed for preloading vs postloading in panels B and C. In panels D−F, Spearman correlation analysis was performed to assess the relationship between the number of anthracycline molecules per MB and the drug properties. * and ** represent $p < 0.05$ and $p < 0.01$, respectively.

At the higher feed ratio of 2:1, preloading resulted in significantly higher drug loading for several anthracyclines, including idarubicin, daunorubicin, and valrubicin (Figure 3C). With the exception of valrubicin, however, for which more than 100-fold increased loading was achieved, the overall difference was similar for the other five anthracyclines, around 2−3 fold (Figure 3B,C). This enhancement for preloading likely resulted from saturation of the HSA drug binding pockets prior to the formation of drug-loaded HSA MBs. For postloading, HSA is first sonicated to form unloaded HSA MBs. This may result in steric hindrance with regard to access to HSA drug binding pockets, as well as to a certain degree of denaturation or misfolding, thereby compromising subsequent drug loading.[20,21] Furthermore, in the case of postloading, the drug will likely be less optimally associated with HSA MBs because of somewhat reduced access to HSA drug binding pockets. Consequently, the drug can leak out and bind to free HSA during the washing steps. This will likely result in less efficient drug retention in the MB shell and in relatively unstable drug-loaded HSA MBs in the case of the postloading strategy. These factors are considered to be responsible for the higher loading and efficient retention of anthracyclines into the HSA MB shell when employing preloading vs postloading. We furthermore studied if MB formulations with low, medium, and high drug content generated US contrast. Although we observed a decrease in US contrast for MB formulation with the highest level of drug loading, all MB formulations were found to be detectable via US imaging upon drug loading (Figure S2).

We next evaluated the impact of the anthracyclines' physicochemical properties on their loading capacity in the HSA MB shell. For this purpose, we correlated drug loading with binding percentage to albumin (%), hydrophobicity (log *P*), and molecular weight (Da). As shown in Figure 3D, we found that anthracycline loading correlated very well with binding percentage to albumin ($r = 1.00$, $p < 0.01$). The correlations with hydrophobicity and molecular weight were substantially lower (Figure 3E,F). These findings demonstrate that anthracycline with a high binding percentage to albumin confers an advantage with regard to efficient drug loading into the shell of HSA MBs.

It is important to assess if the newly generated anthracycline-loaded HSA MBs can be employed at therapeutically meaningful concentrations. Calculations demonstrate that anthracyclines with low albumin binding and relatively inefficient MB shell loading (i.e., idarubicin, daunorubicin, doxorubicin, and epirubicin) can at best be administered in vivo upon MB formulation at doses around 0.1−1 mg/kg, which is well below their maximum tolerated dose of 5 mg/kg. Employing the preloading strategy and anthracyclines with

https://doi.org/10.1021/acsbiomaterials.1c01203
ACS Biomater. Sci. Eng. XXXX, XXX, XXX−XXX

high albumin binding (i.e., pirarubicin and valrubicin) does result in MB formulations that can be administered in vivo at concentrations in the range of 1−10 mg/kg. These findings underline the importance of selecting the right loading strategy and the right drug to ensure that HSA MB-mediated drug delivery to tumors has a good chance of therapeutic success.

CONCLUSION

We demonstrate that drug loading into the shell of HSA MBs can be maximized by (1) incubating drugs with HSA prior to MB preparation and (2) employing drugs that have a high binding percentage to albumin. Together, these findings showcase that the drug loading strategy and the drugs' physicochemical properties play key roles in the development of highly efficiently loaded HSA MBs. The resulting anthracycline-loaded MBs are considered to be useful for US-based image-guided and triggerable drug delivery to tumors, which is becoming increasingly popular.[22,23]

MATERIALS AND METHODS

Materials. Daunorubicin, doxorubicin, and epirubicin were purchased from LC Laboratories (US). Idarubicin and pirarubicin were bought from AbMole BioScience (US). Valrubicin was obtained from United States Pharmacopeia (USA). Human serum albumin (HSA), dextrose, and sodium chloride were bought from Rocky Mountain Biologicals (US), Carl Roth (Germany), and Sigma-Aldrich (Germany), respectively. Perfluorobutane was obtained from abcr GmbH (Germany). Deionized (DI) water was used for all experiments. All reagents were of appropriate analytical grade.

Synthesis and Stability of HSA MB. HSA MBs were prepared using a similar protocol as described in the literature.[3] To prepare the HSA stock solution, we added 5% (w/v) HSA, 0.9% (w/v) sodium chloride, and different concentrations of dextrose: 5, 10, and 15% (w/v) to 5 mL of DI water in a V-shaped rotary flask. Upon addition, the mixture was saturated with perfluorobutane gas. Subsequently, the solution was sonicated twice with a 20 kHz Bandelin ED241 device (Bandelin Electronic, Berlin, Germany) at 100% ultrasound amplitude for 2 min with a gap of 10 s. The formed MBs were allowed to float because of their buoyancy, and the solution underneath was replaced multiple times to remove the unreacted solutes. Finally, the HSA MBs were suspended in 3% (w/v) HSA and stored at room temperature (RT) for further use. To study the stability, we stored HSA MBs in screw-cap glass vials at RT. Particularly, the size and concentration of HSA MBs were evaluated using a Multisizer 3 (Beckmann Coulter, Germany) over a period of 4 weeks as described previously.[16]

Bright-Field Microscopy. To enable the qualitative assessment of the size and shape of HSA MBs, we employed an Axio Imager M2 fluorescence microscope equipped with an AxioCam MRm Rev.3 camera (Carl-Zeiss, Oberkochen, Germany). We placed a drop of the sample on an histobond adhesive microscope slide (Paul Marienfeld GmbH & Co.KG, Lauda-Königshofen, Germany) and measured it in bright-field mode. The images were acquired with a magnification of 40×.

US Properties of HSA MB. To investigate the US properties of HSA MB, we employed a preclinical US device (Vevo 2100, VisualSonics, Canada) to visualize the contrast generated from HSA MBs. To this end, 1×10^8 MBs were diluted in 4.5 mL of DI water containing 3% (w/v) HSA, and the mixture was added into 10% (w/v) gelatin phantoms. The gelatin phantoms employed are a mixture of gelatin and water. Such phantoms are widely employed in ultrasound imaging studies because of their ease of preparation, cost-effectiveness, and their ability to mimic the acoustic properties of soft tissues.[24] The phantoms were imaged in both brightness-mode (B-mode) and nonlinear contrast mode (C-mode) at 18 MHz center frequency and 4% power (mechanical index 0.2). A region-of-interest was drawn at the center of all images and the resulting contrast intensity was analyzed using the Vevo LAB software. The signal intensity generated from the region-of-interest was used to compare the US properties between HSA MBs in 3% (w/v) HSA and control, i.e., 3 % (w/v) HSA in DI water without any MBs being present.

Quantification of Anthracycline Binding Percentage to Albumin. Ten microliters of 4% (w/v) of the drug solution in DMSO was mixed with 0.5 mL of DI water containing 5% (w/v) HSA and the mixture was incubated at 37 °C for 30 min. The mixture was centrifuged at 500 rpm for 10 min to remove the precipitate. The supernatant containing the unbound dissolved drug and drug−albumin conjugate were centrifuged using a 10 000 MWCO Ultrafilter tube at 12 000 g for 10 min. This step enabled the separation of the unbound dissolved drug from the drug−albumin conjugate. We evaluated the initial drug concentration in albumin solution, supernatant concentration containing the unbound dissolved drug, and drug-albumin conjugate, and the filtrate concentration containing the unbound dissolved drug in triplicate by TECAN Infinite M200 Pro (Tecan Group Ltd., Germany). Details of the experimental parameters used in the TECAN plate reader analysis are summarized in Table S1. Finally, the drug binding percentage to albumin was calculated using the equation

$$\%\text{drug bound to albumin} = \frac{\text{supernatant concentration} - \text{filtrate concentration}}{\text{initial drug concentration}} \times 100\% \quad (1)$$

Drug Loading into the Shell of HSA MB. To prepare drug-loaded HSA MBs, we prepared 2 and 4% (w/v) drug stock solutions and loaded them in the shell of HSA MBs using preloading and postloading strategies. For the preloading strategy, 100 μL of 2 and 4% (w/v) drug solutions in DMSO were added to 5 mL of DI water containing 5% (w/v) HSA and the mixture was incubated for 30 min. This is equivalent to molar concentrations (in mM) of 0.8 and 1.6, 0.7 and 1.4, 0.7 and 1.4, 0.6 and 1.2, and 0.6 and 1.2 for idarubicin, daunorubicin, doxorubicin, epirubicin, pirarubicin, and valrubicin, respectively. Subsequently, the mixture was saturated with perfluorobutane gas and sonicated in the same way as described in the section Synthesis and Stability of HSA MB. On the contrary, in the postloading strategy, unloaded HSA MBs were synthesized and incubated with 100 μL of 2 and 4% (w/v) drug solutions for 30 min. Finally, the drug-loaded HSA MBs were allowed to float because of their buoyancy and the solution underneath was replaced multiple times to remove the precipitates and the dissolved constituents. Finally, the HSA MBs were suspended in 3% (w/v) HSA and stored at RT for further use.

Quantification of Drug Loading in the Shell of HSA MBs. Drug-loaded HSA MBs were destroyed and the encapsulated drug was released by adding 10 μL of drug-loaded HSA MBs to 90 μL of DMSO. The concentration of the encapusulated drug in the MB shell was determined with TECAN Infinite M200 Pro (Tecan Group Ltd., Germany). The number of drug molecules per HSA MB was calculated as

$$\#\text{of drug molecules/HSA MB} = \frac{\text{concentration of the encapsulated drug}}{\text{molecular weight of the drug}} \times \frac{\text{Avogadro's number}}{\text{MB concentration}} \quad (2)$$

Statistical Analysis. Three different batches of unloaded and drug-loaded HSA MB formulations were prepared and each formulation was measured thrice. All values are presented as mean ± standard deviation. Statistical analyses were performed using *GraphPad Prism 9*. The results in panels A and B in Figure 2 were analyzed using two-way ANOVA, corrected for multiple comparisons (Bonferroni), whereas Figures 2E and 3B,C were analyzed using multiple *t* tests. The correlation analyses in Figure 3D−F were performed using Spearman r correlation. A p value of less than 0.05 was considered to be statistically significant.

https://doi.org/10.1021/acsbiomaterials.1c01203
ACS Biomater. Sci. Eng. XXXX, XXX, XXX−XXX

■ ASSOCIATED CONTENT

Supporting Information

The Supporting Information is available free of charge at https://pubs.acs.org/doi/10.1021/acsbiomaterials.1c01203.

Size distribution of HSA MBs (Figure S1); contrast-mode US imaging of HSA MBs loaded with low, medium, and high levels of anthracyclines (Figure S2); experimental parameters for anthracycline analysis using fluorescence spectroscopy (Table S1) (PDF)

■ AUTHOR INFORMATION

Corresponding Author

Twan Lammers − *Institute for Experimental Molecular Imaging, RWTH Aachen University Clinic, Aachen 52074, Germany;* orcid.org/0000-0002-1090-6805; Email: tlammers@ukaachen.de

Authors

Mengjiao Liu − *Institute for Experimental Molecular Imaging, RWTH Aachen University Clinic, Aachen 52074, Germany*

Anshuman Dasgupta − *Institute for Experimental Molecular Imaging, RWTH Aachen University Clinic, Aachen 52074, Germany*

Na Qu − *Liaoning University, Shenyang 110036, China*

Elena Rama − *Institute for Experimental Molecular Imaging, RWTH Aachen University Clinic, Aachen 52074, Germany*

Fabian Kiessling − *Institute for Experimental Molecular Imaging, RWTH Aachen University Clinic, Aachen 52074, Germany;* orcid.org/0000-0002-7341-0399

Complete contact information is available at: https://pubs.acs.org/10.1021/acsbiomaterials.1c01203

Author Contributions

†M.L and A.D. contributed equally.

Notes

The authors declare no competing financial interest.

■ ACKNOWLEDGMENTS

This work was supported by the Chinese Scholarship Council (grant 201506910070), the European Commission (Euro-NanoMed-III: NSC4DIPG), the European Research Council (ERC-CoG 864121), and the German Research Foundation (DFG: GRK 2375 (grant 331065168) and SFB 1066).

■ REFERENCES

(1) Li, Y.; Chen, Y.; Du, M.; Chen, Z. Y. Ultrasound technology for molecular imaging: from contrast agents to multimodal imaging. *ACS Biomater. Sci. Eng.* **2018**, *4* (8), 2716−2728.

(2) Sirsi, S. R.; Borden, M. A. Microbubble compositions, properties and biomedical applications. *Bubble Sci., Eng., Technol.* **2009**, *1* (1−2), 3−17.

(3) Borrelli, M. J.; O'Brien, W. D., Jr; Bernock, L. J.; Williams, H. R.; Hamilton, E.; Wu, J.; Oelze, M. L.; Culp, W. C. Production of uniformly sized serum albumin and dextrose microbubbles. *Ultrason. Sonochem.* **2012**, *19* (1), 198−208.

(4) Du, M.; Chen, Y.; Tu, J.; Liufu, C.; Yu, J.; Yuan, Z.; Gong, X.; Chen, Z. Ultrasound responsive magnetic mesoporous silica nanoparticle-loaded microbubbles for efficient gene delivery. *ACS Biomater. Sci. Eng.* **2020**, *6* (5), 2904−2912.

(5) Wu, S. K.; Tsai, C. L.; Huang, Y.; Hynynen, K. Focused ultrasound and microbubbles-mediated drug delivery to brain tumor. *Pharmaceutics* **2021**, *13* (1), 15.

(6) Snipstad, S.; Vikedal, K.; Maardalen, M.; Kurbatskaya, A.; Sulheim, E.; de Lange Davies, C. Ultrasound and microbubbles to beat barriers in tumors: improving delivery of nanomedicine. *Adv. Drug Delivery Rev.* **2021**, *177*, 113847.

(7) Köse, G.; Darguzyte, M.; Kiessling, F. Molecular ultrasound imaging. *Nanomaterials* **2020**, *10* (10), 1935.

(8) Chowdhury, S. M.; Abou-Elkacem, L.; Lee, T.; Dahl, J.; Lutz, A. M. Ultrasound and microbubble mediated therapeutic delivery: Underlying mechanisms and future outlook. *J. Controlled Release* **2020**, *326*, 75−90.

(9) Klibanov, A. L. Ultrasound contrast: Gas microbubbles in the vasculature. *Invest. Radiol.* **2021**, *56* (1), 50−61.

(10) Chandan, R.; Mehta, S.; Banerjee, R. Ultrasound-responsive carriers for therapeutic applications. *ACS Biomater. Sci. Eng.* **2020**, *6* (9), 4731−4747.

(11) Dasgupta, A.; Liu, M.; Ojha, T.; Storm, G.; Kiessling, F.; Lammers, T. Ultrasound-mediated drug delivery to the brain: principles, progress and prospects. *Drug Discovery Today: Technol.* **2016**, *20*, 41−48.

(12) Delaney, L. J.; Eisenbrey, J. R.; Brown, D.; Brody, J. R.; Jimbo, M.; Oeffinger, B. E.; Stanczak, M.; Forsberg, F.; Liu, J. B.; Wheatley, M. A. Gemcitabine-loaded Microbubble System for Ultrasound Imaging and Therapy. *Acta Biomater.* **2021**, *130*, 385−394.

(13) Gao, J.; Logan, K. A.; Nesbitt, H.; Callan, B.; McKaig, T.; Taylor, M.; Love, M.; McHale, A. P.; Griffith, D. M.; Callan, J. F. A single microbubble formulation carrying 5-fluorouridine, Irinotecan and oxaliplatin to enable FOLFIRINOX treatment of pancreatic and colon cancer using ultrasound targeted microbubble destruction. *J. Controlled Release* **2021**, *338*, 358−366.

(14) Ruan, J. L.; Browning, R. J.; Yildiz, Y. O.; Bau, L.; Kamila, S.; Gray, M. D.; Folkes, L.; Hampson, A.; McHale, A. P.; Callan, J. F.; et al. Evaluation of Loading Strategies to Improve Tumor Uptake of Gemcitabine in a Murine Orthotopic Bladder Cancer Model Using Ultrasound and Microbubbles. *Ultrasound med. bio.* **2021**, *47* (6), 1596−1615.

(15) Fokong, S.; Theek, B.; Wu, Z.; Koczera, P.; Appold, L.; Jorge, S.; Resch-Genger, U.; van Zandvoort, M.; Storm, G.; Kiessling, F.; Lammers, T. Image-guided, targeted and triggered drug delivery to tumors using polymer-based microbubbles. *J. Controlled Release* **2012**, *163* (1), 75−81.

(16) Liu, M.; Dasgupta, A.; Koczera, P.; Schipper, S.; Rommel, D.; Shi, Y.; Kiessling, F.; Lammers, T. Drug loading in poly (butyl cyanoacrylate)-based polymeric microbubbles. *Mol. Pharmaceutics* **2020**, *17* (8), 2840−2848.

(17) Keller, M. W.; Glasheen, W.; Kaul, S. Albunex: a safe and effective commercially produced agent for myocardial contrast echocardiography. *J. Am. Soc. Echocardiogr.* **1989**, *2* (1), 48−52.

(18) Clark, L. N.; Dittrich, H. C. Cardiac imaging using Optison. *Am. J. Cardiol.* **2000**, *86* (4), 14−18.

(19) Chen, J. L.; Dhanaliwala, A. H.; Dixon, A. J.; Klibanov, A. L.; Hossack, J. A. Synthesis and characterization of transiently stable albumin-coated microbubbles via a flow-focusing microfluidic device. *Ultrasound med. bio.* **2014**, *40* (2), 400−409.

(20) Stathopulos, P. B.; Scholz, G. A.; Hwang, Y. M.; Rumfeldt, J. A.; Lepock, J. R.; Meiering, E. M. Sonication of proteins causes formation of aggregates that resemble amyloid. *Protein Sci.* **2004**, *13* (11), 3017−3027.

(21) Gülseren, İ.; Güzey, D.; Bruce, B. D.; Weiss, J. Structural and functional changes in ultrasonicated bovine serum albumin solutions. *Ultrason. Sonochem.* **2007**, *14* (2), 173−183.

(22) Koczera, P.; Appold, L.; Shi, Y.; Liu, M.; Dasgupta, A.; Pathak, V.; Ojha, T.; Fokong, S.; Wu, Z.; Van Zandvoort, M.; et al. PBCA-based polymeric microbubbles for molecular imaging and drug delivery. *J. Controlled Release* **2017**, *259*, 128−135.

(23) Sun, T.; Dasgupta, A.; Zhao, Z.; Nurunnabi, M.; Mitragotri, S. Physical triggering strategies for drug delivery. *Adv. Drug Delivery Rev.* **2020**, *158*, 36−62.

(24) Amidi, E.; Yang, G.; Uddin, K. S.; Wahidi, R.; Zhu, Q. Low-cost ultrasound and optical gelatin-based phantoms. *Proc. SPIE* **2019**, *10878*, 157.

https://doi.org/10.1021/acsbiomaterials.1c01203
ACS Biomater. Sci. Eng. XXXX, XXX, XXX−XXX

-Supplementary information-

Strategies to Maximize Anthracycline Drug Loading in Albumin Microbubbles

Mengjiao Liu[1,#], Anshuman Dasgupta[1,#], Na Qu[2], Elena Rama[1],

Fabian Kiessling[1], Twan Lammers[1,*]

[1] Institute for Experimental Molecular Imaging, RWTH Aachen University Clinic, Forckenbeckstrasse 55, 52074 Aachen, Germany.

[2] Liaoning University, No. 66 Chongshan Middle Road, Huanggu District, Shenyang 110036, China.

[#] Both authors contributed equally.

* Corresponding author: tlammers@ukaachen.de.

Number of pages: 4

Number of figures: 2

Number of tables: 1

Figure S1

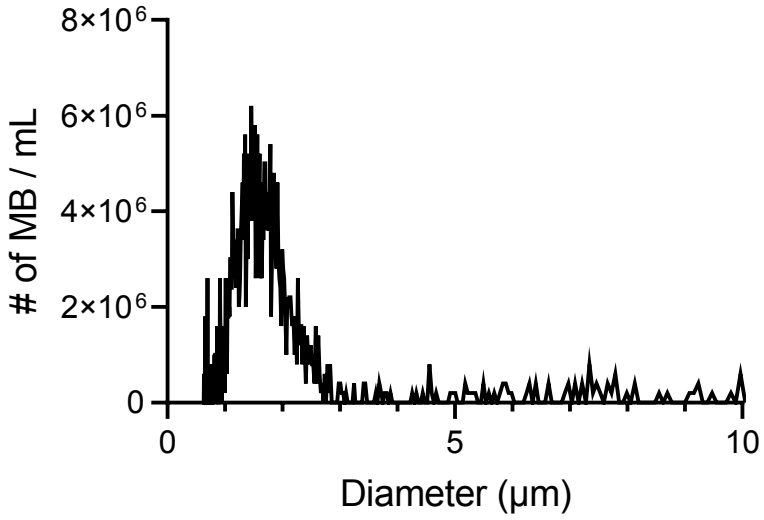

Figure S1. Size distribution of HSA MB. Coulter counter results show that HSA MB has a relatively broad size distribution.

Figure S2

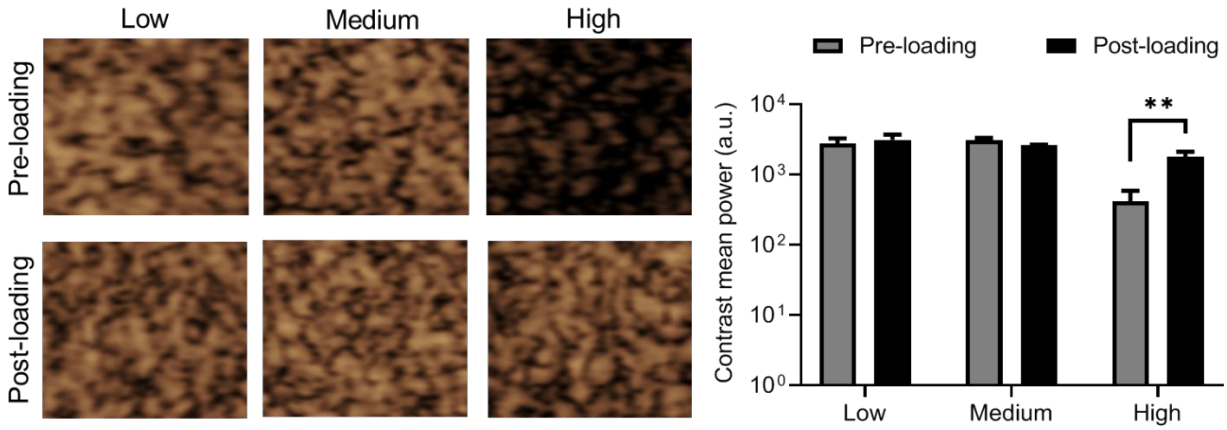

Figure S2. Contrast-mode US imaging of HSA MB loaded with low, medium and high levels of anthracyclines. Qualitative and quantitative analyses showing that all MB formulations generate US contrast upon anthracycline loading. Low, medium and high refers to the levels of anthracycline loaded in HSA MB. Low = idarubicin, medium = doxorubicin and high = valrubicin.

Table S1

Drug	Parameter
Idarubicin	Excitation Wavelength 478 nm, Emission Wavelength 572 nm
Daunorubicin	Excitation Wavelength 498 nm, Emission Wavelength 596 nm
Doxorubicin	Excitation Wavelength 498 nm, Emission Wavelength 596 nm
Epirubicin	Excitation Wavelength 498 nm, Emission Wavelength 596 nm
Pirarubicin	Excitation Wavelength 498 nm, Emission Wavelength 596 nm
Valrubicin	Excitation Wavelength 498 nm, Emission Wavelength 596 nm

Table S1. Experimental parameters for anthracycline analysis using fluorescence spectroscopy.

Acknowledgements

Finally, I have reached the most readable part of my thesis. To be honest, I have spent a considerable amount of time thinking about this section, but I still haven't found the perfect way to articulate it.

During my entire PhD journey, Professor Twan Lammers and professional Anshuman Dasgupta have been the two most valuable individuals.

First and foremost, I would like to express my sincere gratitude to my supervisor, Professor Twan Lammers. You have been a guiding light and a constant source of support throughout my academic path. Your profound knowledge, exceptional talent, and rigorous scholarly attitude have played a decisive role in my academic growth. Not only have you patiently guided and nurtured me academically, but you have also provided invaluable guidance and support in my personal life. I am forever grateful for your teachings and dedication. Your Chinese name, which means special and knowledgeable, truly reflects your character.

I would also like to extend my deep appreciation to professional Anshuman Dasgupta. Working with you has been one of the most enjoyable experiences during my doctoral career. Your intelligence, diligence, and team spirit have inspired me to strive constantly and surpass my own expectations. We have spent countless nights together, solving one research problem after another, and shared many joys and challenges. Because of you, I have experienced the warmth of friendship and the power of collaboration. Your motto, "you make your own luck," has been a great source of encouragement. Thank you for your companionship and support.

I cannot forget to thank Dr. Kose, who has had a significant impact on my life. Whenever I faced difficulties, you were always ready to lend a helping hand. You are truly a deserving true friend. Thank you for your constant encouragement and supervision, which made me feel less afraid and lonely in times of helplessness. You deserve a bright future. Thank you.

How could I overlook my beloved friends? Bi, Junlin, and Yuchen, we have shared so many wonderful memories together, especially during our trip to Phantasialand. That

journey will remain etched in my memory forever. Cindy and Sam, you two are my best friends. We have known each other for about 10 years, and you hold a special place in my heart. Na, I wish you the best of luck in China. The year you spent with me in Germany was fantastic. Leiming, I also want to thank you for your help in organic chemistry. I have truly learned a lot from you. Elena, you are a lovely Italian girl, and I appreciate your kindness. I still remember our plan to visit your beautiful dolphins' hometown. Armin, you are the most gentle person I have ever met. It is my good fortune to know you, and I truly enjoy our conversations. Diana and Marek, thank you for your tremendous help in the lab. Dirk, thank you for assisting me with capturing our microbubble images in DWI. I hope you can attend my defense. Sandra and Patrick, I am grateful for your suggestions regarding the revision of our microbubble paper.

Furthermore, I would like to express my gratitude to Prof. Fabian Kiessling for providing me with the opportunity to study at ExMI. Your approach to science has been truly inspiring. I would also like to thank Prof. Yang Shi for guiding me and offering valuable advice.

Lastly, I want to thank my family. You have been my unwavering support and strongest advocates throughout this journey. Your unconditional love and trust have propelled me forward, helping me overcome many difficulties and challenges. I am profoundly grateful for everything you have sacrificed for me.

Mengjiao

Affidavit according to § 5 (1) for Data Retention

Hiermit erkläre ich, dass die dieser Dissertation zu Grunde liegenden Originaldaten im Institut für Experimentelle Molekulare Bildgebung des Universitätsklinikums Aachen hinterlegt sind.

Mengjiao Liu

Affidavit according to § 5 (1) and (2), and § 11 (3) 12 of the doctoral studies regulations

I hereby declare on oath, **Mengjiao Liu**, that I have contributed a significant part, and thus majority, of the publication: **Liu, M.***, Dasgupta, A.*, Koczera, P., Schipper, S., Rommel, D., Shi, Y., Kiessling, F. and Lammers, T.: Drug Loading in Poly(butyl cyanoacrylate)-Based Polymeric Microbubbles; Molecular Pharmaceutics; 2020 August 03; 17(8): 2840–2848.

The contributions to the publication were as follows:

	Liu, M.	Dasgupta, A.	Koczera, P.	Schipper, S.	Rommel, D.	Shi, Y.	Kiessling, F.	Lammers, T.	Sum (%)
Study supervision		30						70	100
Study design	55	35						10	100
Performing experiments	55	40			5				100
Data evaluation	55	40						5	100
Statistical evaluation	55	45							100
Interpretation of data evaluation	55	40					5		100
Writing/draft of the manuscript	100								100
Correction of the manuscript		50	5	5	5	5		30	100

The position as the first author obviously arises from this significant contribution.

_____

Mengjiao Liu

As supervisor and corresponding author I confirm the statements of Mengjiao Liu

_____

Prof. Dr. Dr. Twan Lammers

As co-author I endorse the statement of Prof. Dr. Dr. Twan Lammers

_____ _____

Anshuman Dasgupta Dr. med. Patrick Koczera

_____ _____

Dr. Sandra Schipper Dirk Rommel

_____ _____

Prof. Yang Shi Prof. Dr. med. Fabian Kiessling

Affidavit according to § 5 (1) and (2), and § 11 (3) 12 of the doctoral studies regulations

I hereby declare on oath, **Mengjiao Liu**, that I have contributed a significant part, and thus majority, of the publication: **Liu, M**.*, Dasgupta, A.*, Qu, N., Rama, E., Kiessling, F. and Lammers, T.: Strategies to Maximize Anthracycline Drug Loading in Albumin Microbubbles; ACS Biomaterials Science and engineering; 2021 December 21; A-G.

The contributions to the publication were as follows:

	Liu, M.	Dasgupta, A.	Qu, N.	Rama, E.	Kiessling, F.	Lammers, T.	Sum (%)
Study supervision		30				70	100
Study design	55	20	5			20	100
Performing experiments	55	35	5	5			100
Data evaluation	55	40			5		100
Interpretation of data evaluation	55	40	5				100
Statistical evaluation	55	45					100
Writing/draft of the manuscript	100						100
Correction of the manuscript		50				50	100

The position as the first author obviously arises from this significant contribution.

_____

Mengjiao Liu

As supervisor and corresponding author I confirm the statements of Mengjiao Liu and as a representative of the collaborative partner Dr. Na Qu

_____

Prof. Dr. Dr. Twan Lammers

As co-author I endorse the statement of Prof. Dr. Dr. Twan Lammers

_____ _____

Anshuman Dasgupta Elena Rama

_____

Prof. Dr. med. Fabian Kiessling

Curriculum vitae

Mengjiao Liu

Date of Birth: 01/08/1989

Place of Birth: Wuyang, Henan Province, China

Nationality: People's Republic of China

Address: Kullenhofstrasse 54B, 52074,

Aachen, Germany

Telephone: +49 17637165404

Email: liumengjiao8908@outlook.com

EDUCATION

September 2015-Now Biomedical Engineering, RWTH-Aachen University, Germay (Supervisor: Professor Twan Lammers)

September 2012- June 2015 Pharmacy，College of Veterinary Medicine, Sichuan Agricultural University, P. R. China (Supervisor: Professor Hualin Fu)

September 2008-June 2011 Animal Husbandry, Henan University of Animal Husbandry and Ecomony, P. R. China

HONOR/AWARD

National Scholarship for Graduate Students

Outstanding graduate student of Sichuan Province

Excellent Master's Thesis Cultivation Fund

LANGUAGE

Chinese Mother Tongue

English Fluent

German A2

PUBLICATIONS

- Dasgupta, A., Sun, T., Palomba, R., Rama, E., Zhang, Y., Power, C., Moeckel, D., **Liu, M.**, et al., Nonspherical ultrasound microbubbles. Proceedings of the National Academy of Sciences, 2023.
- **Liu, M.***, Dasgupta, A.*, et al., Maximizing Anthracycline Drug Loading in Albumin Microbubbles. ACS Biomaterials Science and engineering, 2021.

- **Liu, M.*,** Dasgupta, A.*, et al., Drug loading in poly (butyl cyanoacrylate)-based polymeric microbubbles. Molecular Pharmaceutics, 2020.
- Fernandes, A.C.*, **Liu, M.***, et al., A computational and experimental study to develop E-selectin targeted peptides for molecular imaging applications. Future medicinal chemistry, 2018.
- Koczera P., Appold L., Shi Y., **Liu M.**, et al.**,** PBCA-based polymeric microbubbles for molecular imaging and drug delivery. Journal of Controlled Release, 2017.
- Dasgupta, A., **Liu, M.**, et al., Ultrasound-mediated drug delivery to the brain: principles, progress and prospects. Drug Discovery Today: Technologies, 2016.
- Lu, C., **Liu, M.*,** et al., Novel thermosensitive in situ gel based on poloxamer for uterus delivery. European Journal of Pharmaceutical Sciences, 2015.
- **Liu, M.**, Yin, D., et al. Solid–liquid equilibrium of azithromycin in water + 1,2-propanediol solutions from (289.35 to 319.15) K. Journal of Molecular Liquids, 2014.
- **Liu, M.**, Fu, H., et al. Measurement and Correlation of the Solubility of Enrofloxacin in Different Solvents from (303.15 to 321.05) K. Journal of Chemical & Engineering Data, 2014.
- **Liu, M.**, Fu, Q., et al. et al. A New Kinetic Approach. Stability of Cefquinome Sulfate under Variable pH and Temperature[J]. Indian Journal of Pharmaceutical Education and Research, 2014.
- **Liu, M.**, Fu, H., et al. Preparation of cefquinome sulfate liposome. Guocheng Gongcheng Xuebao/The Chinese Journal of Process Engineering, 2013.